F. Chen

SOLE COPY F. CHEN

# The Behavior of Langmuir Probes in Time-Varying Situations

by

Francis F. Chen

MATT-269 June, 1964

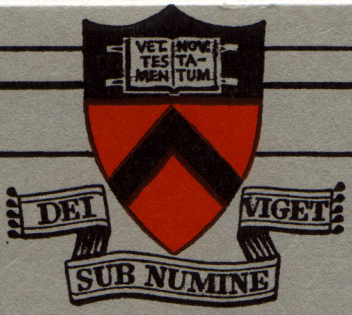


PLASMA PHYSICS LABORATORY

Contract AT(30-1)—1238 with the
US Atomic Energy Commission

PRINCETON UNIVERSITY
PRINCETON, NEW JERSEY

Princeton University
Plasma Physics Laboratory
Princeton, New Jersey

# The Behavior of Langmuir Probes in Time-Varying Situations

by

Francis F. Chen

MATT-269 June, 1964

AEC RESEARCH AND DEVELOPMENT REPORT

This work was supported under Contract AT(30-1)-1238 with the Atomic Energy Commission. 

# The Behavior of Langmuir Probes in Time-Varying Situations

by

Francis F. Chen
Plasma Physics Laboratory, Princeton University,
Princeton, New Jersey

## ABSTRACT

In the past two years a number of papers have appeared which have to do with the hitherto ill-explored subject of the behavior of electrostatic probes and sheaths in time-dependent situations. The present work, which is actually chapter 6 of a forthcoming book on electrostatic probes, analyzes, summarizes, and in some cases extends what is presently known about this subject. This report is being issued at this time because the results contained herein may be of immediate importance to diagnostic measurements in this laboratory and may also suggest a number of interesting research topics. In particular, Sec. 6.1 concerns the validity of probe temperature measurements in noisy plasmas; Sec. 6, 2 concerns a new technique for density measurements in plasmas too small for ordinary microwave interferometry; and Sec. 6. 3 concerns the ultimate speed with which probe measurements can be made. Finally, Sec. 6. 4 is an introduction to the technique of correlation measurements developed in this laboratory and may be helpful to others who wish to study turbulance in plasmas.

# 6. TIME-DEPENDENT PHENOMENA

Up to now we have been concerned with measurements which are essentially steady state. We now consider what happens to the probe current when either the plasma parameters or the probe potential fluctuates. In many instances the plasma being studied will not be quiescent; time-averaged probe characteristics then may or may not give accurately the average plasma properties. This problem will be considered in Sec. 6.1. A similar problem occurs when the probe potential is varied in a steady plasma. New measurement techniques then become possible. We have already seen in Sec. 3.2.4 how the electron velocity distribution can be measured by applying an ac signal to the probe; in Sec. 6.2 we shall discuss the technique of the resonance probe, in which a signal near the electron plasma frequency is used.

In Sec. 6.3 we shall discuss the response of a probe to a voltage pulse. Since this response is controlled by the relatively slow motion of the ions, this problem is the same as that of applying a signal near the ion plasma frequency to the probe. The importance of this problem is felt when a sawtooth voltage pulse is applied to a probe to obtain the entire characteristic in a short time of the order of a microsecond. This is desirable under the following circumstances. First, in low-temperature plasmas the contact potential between the probe and the plasma is important, and it is necessary to obtain the probe characteristic before the contact potential is changed by the deposition of impurities on the probe surface. Second, in unsteady plasmas the time during which the plasma parameters are constant may be quite short. Third, in intense

discharges a probe may melt when it draws a large electron current; by keeping it near $V_f$ and pulsing it, one can use the heat capacity of the probe to keep it from melting during the voltage sweep. Finally, in the measurement of velocity distributions (Sec. 3.2.4) it is possible to obtain $dI/dV$ or $d^2I/dV^2$ by pulsing the probe voltage and time-differentiating the probe current by RC networks. In addition, probes are often used to measure oscillations and fluctuations in a plasma. In all these applications one assumes that the probe sheath is in equilibrium with the plasma at all times. It is therefore important to know the frequency response of a probe and its sheath.

Finally, in Sec. 6.4, we shall describe the use of probes to measure correlation functions in fluctuating plasmas.

## 6.1 Effect of Oscillations on DC Probe Characteristics

The effect of fluctuations in $n$, $kT_e$, $V_p$, and $V_s$ on the time-averaged I - V characteristic obtained the usual way has been investigated by Garschadden and Emeleus ( 1 ), Crawford ( 2 ), Boschi and Magistrelli ( 3 ), and Sugawara and Hatta ( 4 ). The result is relatively simple when the probe is biased to the transition region of the characteristic and the fluctuations do not take the probe out of this region. The electron flux density to the probe is then given by

$$j_{eo} = j_r e^{-\eta} \quad , \tag{6.1-1}$$

where, as usual,

$$j_r = n(kT_e/2\pi m_e)^{\frac{1}{2}} \qquad (6.1\text{-}2)$$

and

$$\eta = -e(V_p - V_s)/kT_e \quad . \qquad (6.1\text{-}3)$$

Now let the density be given by $n + \tilde{n}$, the temperature by $kT_e + k\tilde{T}_e$, and so forth, where the tilde indicates the time-varying component. Because of the non-linearity of Eq. (6.1-1), the average value $\langle j_e \rangle$ of $j_e$ will then in general be different from $j_{eo}$, the value of $j_e$ when each fluctuating quantity is replaced by its average value. This difference will depend on $\tilde{n}$, $k\tilde{T}_e$, $\tilde{V}_p - \tilde{V}_s$ as well as on the cross-correlations among them. A linearized treatment of the general case has been given by Crawford ( 2 ).

Let us consider first the case when $kT_e$ does not vary. We may then introduce $\tilde{\eta}$ and write

$$j_e = j_{eo}(1 + \tilde{j}_r/j_r)\exp(-\tilde{\eta}) \quad . \qquad (6.1\text{-}4)$$

With the use of Eq. (6.1-2), the average value is given by

$$\langle j_e \rangle = j_{eo}\langle (1 + \tilde{n}/n)\exp(-\tilde{\eta})\rangle \quad . \qquad (6.1\text{-}5)$$

From this equation we may draw two important conclusions. First, if $\tilde{\eta}$ vanishes, we have $\langle j_e \rangle = j_{eo}$ since $\langle \tilde{n} \rangle$ is zero; density fluctuations alone do not affect the characteristic. Second, since $V_p$ occurs only in $j_{eo}$, we have $d\ell n \langle j_e \rangle / dV_p = d\ell n\, j_{eo}/dV_p$. Hence determinations of $kT_e$ from the $\ell n\, I_e - V_p$ curve are unaffected by fluctuations in $n$ and $V_p$ or $V_s$ regardless of their amplitude, as long as the exponential law (6.1-1) is obeyed.

When $\tilde{n}$ is zero and $\tilde{\eta}$ is given by $\delta\eta \cos \omega t$, the integration indicated in Eq. (6.1-5) can be carried out to obtain

$$\langle j_e \rangle = j_{eo} I_o ( \delta\eta) \quad , \tag{6.1-6}$$

where $I_o$ is a Bessel function of imaginary argument. Note that $\langle j_e \rangle$ is independent of frequency. This result was first obtained by Kojima et. al. ( 5 ) and has been verified by a number of authors over a large range of frequencies. For instance, in Fig. 6.1 we show the data of Garschadden and Emeleus ( 1 ) taken by imposing a sinusoidal voltage on the probe. It is clear that the $\ell n$ I - V curve is merely shifted upwards by a constant, retaining the same slope. Since the saturation regions are relatively unaffected, this shift necessitates a rounding of the "knee" of the curve and introduces some uncertainty in the determination of $V_s$ and of saturation electron current. In Fig. 6.2 we show the data of Cairns ( 6 ) verifying the $I_o$ dependence of $\langle j_e \rangle$ on $\delta\eta$. By fitting curves of $I_o$ to the data, the argument of $I_o$ can be found; this provides another method of determining $kT_e$.

Fig. 6.1

Fig. 6.2

When $\tilde{\eta}$ and $\tilde{n}$ occur simultaneously, and $\tilde{n}$ is given by $\delta n \cos(\omega t + \phi)$, Eq. (6.1-5) yields

$$\langle j_e \rangle = j_{eo} \left[ I_o(\delta\eta) - n^{-1} \delta n \cos\phi \, I_1(\delta\eta) \right] . \tag{6.1-7}$$

The second-order cross-modulation term has been verified experimentally by Crawford ( 2 ), who produced the density and potential fluctuations by modulating the discharge current and the probe potential simultaneously with a variable phase shift.

We now consider the more complicated case when $kT_e$ fluctuates but n, $V_p$, and $V_s$ are constant. If $k\tilde{T}_e$ is the time-varying part of $kT_e$, Eq. (6.1-1) can be written

$$j_e = n(2\pi m_e)^{-\frac{1}{2}} (kT_e + k\tilde{T}_e)^{\frac{1}{2}} \exp\left[e(V_p - V_s)/(kT_e + k\tilde{T}_e)\right] . \qquad (6.1\text{-}8)$$

Assuming $k\tilde{T}_e/kT_e \equiv \epsilon f(t) << 1$, we may expand Eq. (6.1-8) to obtain, to second order in $\epsilon$,

$$j_e = j_{eo}\left[1 + (\tfrac{1}{2} + \eta)\,\epsilon f - \tfrac{1}{2}(\tfrac{1}{4} + \eta - \eta^2)\,\epsilon^2 f^2\right] . \qquad (6.1\text{-}9)$$

For $f(t) = \cos \omega t$, the average value is

$$\langle j_e \rangle = j_{eo}\left[1 - \tfrac{1}{4}\epsilon^2(\tfrac{1}{4} + \eta - \eta^2)\right] . \qquad (6.1\text{-}10)$$

Note that $\eta$ appears in the correction factor, so that the slope of the ln I - V curve is affected by fluctuations in $kT_e$. The simple expression (6.1-10) could be obtained only by linearizing; fortunately, fluctuations in $kT_e$ are rarely important experimentally. Detailed observations of the effects of different types of fluctuations, including those with square and sawtooth waveforms, have been made by Sujawara and Hatta ( 4 ).

When the oscillations in potential bring the probe into the saturation regions of the characteristic, the result is no longer independent of the shape of the probe, as it is in the transition region. The effect on positive probes operating in the

orbital-motion regime has been discussed by Garschadden and Emeleus ( 1 ). The effect on negative probes spending part of the cycle in the saturation ion current region has been studied thedretically and experimentally by Boschi and Magistrelli ( 3 ). Their results are shown on Fig. 6.3. In obtaining the theoretical curves these authors used the Bohm formula (3.3-1) for ion current to a plane probe and took into account the fraction of each cycle a probe with a superimposed sinusoidal potential would spend in the saturation ion region. The shift of floating potential is clearly seen from Fig. 6.3. The experimental points agree well near $V_f$ but deviate considerably from theory for large $j_e$. This was attributed primarily to the disturbance of the plasma by the probe; for this reason, Boschi and Magistrelli conclude that this method cannot be used near space potential, although near $V_f$ it is more accurate than the dc method for determining n, $kT_e$, and $V_s$.

Fig. 6.3

In all the experiments mentioned above, a fluctuation in $\eta$ was produced by imposing a signal on the probe. Measurements have also been made in the more realistic but equivalent situation in which the probe bias is fixed and the plasma potential fluctuates. Kojima et. al. ( 5 ) have used a double probe in an rf discharge to measure the local rf field strength $\delta\eta$ by determining the argument of $I_o$ in Eq. (6.1-6). Chen ( 7 ) has used a time-resolved double-probe method, to be described in Sec. 7.1, to determine the effect on apparent $kT_e$ of large-amplitude fluctuations in both $V_s$ and n, extending into the saturation ion region, which commonly occur in practice in discharges in strong magnetic fields. The value of $kT_e$ was found to be unaffected by the fluctuations to within the experimental accuracy of 10%.

Measurements of $\langle j_e \rangle$ with a large sinusoidal voltage on the probe were made by Cairns ( 6 ) and by Ikegami and Takayama ( 8 ) as a function of the dc probe bias. As expected, a peak in $\langle j_e \rangle$ was found when $V_p$ was approximately centered in the transition region of the I - V curve. For values of $V_p$ below this value, accurate determinations of $kT_e$ could be made from Eq. (6.1-6). However, when the excursions in $V_p$ reached into the saturation electron current region, Eq. (6.1-6) gave very large values of $kT_e$.

As pointed out by Ikegami and Takayama, $kT_e$ can be found simply by noting the change $\delta\eta_f$ in floating potential when an oscillation of amplitude $\delta\eta$ is put on the probe. Without the signal, one has

$$j_i = j_r \exp(-\eta_f) \quad . \tag{6.1-11}$$

Since $j_i$ is relatively constant, Eq. (6.1-6) gives in the presence of a signal

$$j_i = j_r \exp(-\eta_f - \delta\eta_f) I_o(\delta\eta) \quad . \tag{6.1-12}$$

Thus

$$I_o(\delta\eta) = \exp(\delta\eta_f) \quad . \tag{6.1-13}$$

For small signals this can be expanded to give the electron temperature:

$$\frac{kT_e}{e} = -\frac{1}{4}\frac{(\delta V)^2}{\delta V_f} \quad . \tag{6.1-14}$$

This change in floating potential has been invoked by Butler and Kino ( 9 ) to explain the constriction of a discharge by a large rf signal applied to a metallic ring surrounding the discharge tube. The inner wall of the tube acts as a floating probe capacitively coupled to the ring and assumes a large negative dc potential, thus creating a thick sheath and constricting the bright portion of the discharge.

## 6.2 Electronic Frequencies: Resonance Probes

In this section we shall discuss the response of a probe to an oscillating potential at frequencies comparable to the electron plasma frequency $\omega_p$. At such high frequencies the ions are too massive to respond to the rf field, and one can assume that the ion motion is unaffected by it. Interest in this subject was initiated by an experiment by Takayama et al. ( 10 ) reported in 1960, in which the time-averaged probe current in the transition region was measured as a function of applied frequency in a very tenuous laboratory plasma. An example of their results is shown in Fig. 6.4.

Fig. 6.4

At low frequencies the increase of $\langle j_e \rangle$ with signal amplitude $\delta V$ is in agreement with that given by Eq. (6.1-6). At some frequency $\omega_r$, there is a resonant peak, beyond which the value of $\langle j_e \rangle$ falls to the dc level. The value of $\omega_r$ did not vary with $\delta V$; and as the density was varied, $\omega_r$ agreed well with the value of $\omega_p$ computed from the saturation electron current. If indeed $\omega_r$ is related to $\omega_p$, this "resonant probe" method can be used to measure plasma density, since it is easy to measure $\omega_r$ with great accuracy. This method would be particularly useful in low-density plasmas, where ordinary microwave techniques fail because the wavelength becomes large compared with the plasma dimensions, and in outer space, where complexity of equipment is at a premium. Unfortunately, the theory of the resonance probe is rather complicated and has been a matter of some recent controversy. Since the entire subject is rather new, the final word is probably yet to come, and we shall present the material in more or less historical order.

The nature of the problem can perhaps be best explained by dividing it into three separate but interrelated problems. Assume that the probe is biased near the floating potential so that the electron distribution is nearly Maxwellian everywhere and that the dc distribution of potential in the sheath and in the quasi-neutral region are known. When an rf voltage is applied to the probe, the first problem (I) is to calculate the distribution of rf field intensity in the sheath and in the plasma. Second, the effect of the field on the electron velocity distribution has to be found (II); this is, of course, related to (I) by a self-consistency requirement. Finally, the effect of the rf velocity component on the dc probe current, or the "resonance rectification", has to be computed (III). The collection of electrons by the probe would also change the velocity distribution, but so far no theory has incorporated this refinement.

### 6.2.1 The Ichikawa-Ikegani Formula

The original theory of Ichikawa and Ikegami ( 11 ) was a heuristic one concerned primarily with problem (II). Thus the externally applied electric field $\tilde{E}_a$ in the plasma was assumed to be $\delta\tilde{V}/L$, where $\delta\tilde{V}$ is the rf potential applied to the probe and $L$ is an adjustable parameter representing an effective screening distance. The sheath was neglected altogether, and the plasma assumed to be homogeneous. By using Poisson's equation and the linearized Boltzmann equation with a simple collision term, and looking for solutions of the form $\exp i(kx - \omega t)$, Ichikawa and Ikegami were able to solve for the perturbation $f_1$ in $f(v)$ and the first-order electric field $E_1$ in terms

of the usual effective dielectric constant. The dc probe current was then taken simply to be

$$j_e = \left\langle \int_{\phi^{\frac{1}{2}}(t)}^{\infty} ev\,[f_o(v) + f_1(v)]\,dv \right\rangle \quad , \tag{6.2-1}$$

evaluated at the probe, where $f_o(v)$ was the Maxwellian distribution and

$$\phi(t) = (2e/m)(V_p + \delta V \sin \omega t) \quad . \tag{6.2-2}$$

From this it is clear that what physically causes resonance rectification is that the oscillation in electron velocity is out of phase with the probe potential at some resonant frequency $\omega_r$, allowing more electrons than usual to overcome the potential barrier, given by Eq. (6.2-2), during the positive half cycle. Note that the sheath makes its appearance only in the term $V_p$ (the sheath drop) in Eq. (6.2-2).. Because of the simplicity of the model, an analytic expression for $\langle j_e \rangle$ could actually be obtained in the limit of long wavelength and small collision frequency $\nu$. This expression reduced to Eq. (6.1-6) in the limit of low and high frequencies and gives a peak at exactly $\omega_p$, corresponding to the excitation of longitudinal plasma oscillations by the rf field. For weakly-ionized gases, the peak height is controlled by collisions with neutral atoms and is given by Ichikawa and Ikegami to be

$$\delta \langle j_e \rangle = \frac{j_{eo}}{2^{3/2}} \frac{\omega_p}{\nu} \frac{h}{L} \eta_p^{\frac{1}{2}}\, \delta\eta\, I_1(\delta\eta) \quad , \tag{6.2-3}$$

where $h$ and $\omega_p$ are the Debye length and electron plasma frequency, $j_{eo}$ and $\eta$ are defined by Eqs. (6.1-1) and (6.1-3), $\delta\eta$ is the normalized rf amplitude applied to the probe, and $I_1$ is a first-order Bessel function. The

full width at half maximum of the peak is given by

$$\delta\omega = 2\nu \quad . \tag{6.2-4}$$

For fully-ionized gases, one sets $\nu = 0$, and the peak height is controlled by Landau damping. The parameter L then appears in $\delta\omega$ instead of $\delta\langle j_e \rangle$:

$$\delta\langle j_e \rangle = j_{eo} 2^{-\frac{1}{2}} \eta_p^{\frac{1}{2}} \delta\eta \; I_1(\delta\eta) \quad , \tag{6.2-5}$$

$$\delta\omega = 4(h/L)^2 \omega_p \quad . \tag{6.2-6}$$

Coulomb collisions were not considered.

The predictions of the Ichikawa-Ikegami theory were verified by Ikegami and Takayama ( 8 ), and more systematically by Cairns ( 6 ) in low-density plasmas with the order of $10^6$ electrons per $cm^3$. Resonance probe curves like those in Fig. 6.4 were taken as a function of discharge current $I_d$ (i.e., plasma density), neutral pressure, signal amplitude, and probe bias. The frequency of resonance varied as $I_d^{\frac{1}{2}}$, which would be in agreement with $\omega_r = \omega_p$. However, the absolute value of n was measured only by means of the saturation electron current, and at low densities considerable uncertainty in this measurement is occasioned by the lack of a well-defined "knee" in the $\ell n$ I-V curve. Thus, it could not be established whether $\omega_r$ was equal to $\omega_p$ or to a constant times $\omega_p$. On the other hand, measurements of the peak height showed the $\delta\eta \; I_1(\delta\eta)$ and $1/\nu$ dependences predicted by Eq. (6.2-3), and the peak width broadened with pressure and was of the magnitude given by Eq. (6.2-4). The parameter L was found to be independent of $\delta\eta$, $\nu$, and n,

as required by the theoretical model, but its magnitude was rather large compared to the Debye length. These authors also measured $\delta\langle j_e\rangle$ as a function of probe bias $\eta_p$ but made no detailed comparison with the theory. Interestingly, Ikegami and Takayama ( 8 ) found that the peak was detectable even with positive probes.

A more severe test of the above theory was made by Peter et al. ( 12 ) in a cesium plasma whose density could be varied between $10^6$ and $10^9$ $cm^{-3}$. The resonance frequency $\omega_r$ was found not to vary as $n_e^{\frac{1}{2}}$ in this range. Furthermore, $\omega_r$ increased with $\eta_p$ – that is, with sheath thickness; this effect was neglected in the Ichikawa-Ikegami theory but will be easily understood in terms of the dielectric slab model. The value of $\omega_r$ was about a factor of 3 below the value of $\omega_p$ given by the knee in the $\ell n$ I-V curve. The variation of $\delta\langle j_e\rangle$ with $\eta_p$ was also measured. Since $j_{eo}$ contains a factor $\exp(-\eta_p)$, Eq. (6.2-3) predicts a peak in $\delta\langle j_e\rangle$ with $\eta_p$. Such a peak was indeed found, but at a much larger value of $\eta_p$ than expected. The variation of $\delta\langle j_e\rangle$ with $\delta\eta$ agreed with Eq. (6.2-3) only for certain values of $\eta_p$, and then only for small values of $\delta\eta$, for which the linear theory was valid.

### 6.2.2 The Dielectric Slab Model

In view of the extreme simplifications used, the agreement of the Ichikawa-Ikegami formula (6.2-3) with experiment is rather remarkable and shows these authors' great insight. The defects of the theory have been summarized by Wimmel ( 13 ) and deal primarily with two points. First is the neglect of the transit time of the electrons from the plasma to the probe;

this introduces an additional phase difference between the electron velocity and the probe potential (problem (III) mentioned above) and will be discussed further in Sec. 6.2.3. Second is the neglect of the sheath region, in which the electron density is not uniform. This affects the rf field in the plasma (problem (I) mentioned above) and will be discussed qualitatively in this section. When the sheath is taken into account, the resonance occurs well below $\omega_p$; instead, the rf field has a minimum at $\omega_p$, as pointed out independently by Levitskii and Shashurin (14), Mayer (15), and Harp (16). That the resonance should occur below $\omega_p$ is easily understood: since $n_e$ is small in the sheath, the average value of $\omega_p$ over the region in which the rf field extends is less than the value of $\omega_p$ in the plasma. To take the sheath inhomogeneity into account will require numerical computation, since it will no longer be possible to Fourier analyze in space; but the main effects can be found from a simple model proposed by Mayer (15) and discussed further by Wimmel (13) and Uramoto et al. (17).

Fig. 6.5

Consider the one-dimensional system shown in Fig. 6.5, consisting of two metal plates with two layers of different dielectric constant $\epsilon$ between them. In the layer representing the sheath, we may set $\epsilon = 1$, since the electron density is negligibly small. In the layer representing the plasma, $\epsilon$ is assumed to be the equivalent dielectric constant of a plasma without a magnetic field:

$$\epsilon = 1 - \omega_p^2/\omega^2 \qquad (6.2\text{-}7)$$

The capacitance per $cm^2$ of the sheath and plasma are then respectively

$$C_s = 1/4\pi s \quad , \quad C_p = \epsilon/4\pi p \quad . \tag{6.2-8}$$

The total impedance seen by the probe is then given by

$$Z = \frac{4\pi}{i\omega}\left(s + \frac{p}{\epsilon}\right) \quad , \tag{6.2-9}$$

and the effective capacitance of the system is

$$C_{eff} = 1/i\omega Z = \frac{\epsilon}{4\pi} \frac{1}{\epsilon s + p} \quad . \tag{6.2-10}$$

The plasma-sheath system therefore has an effective dielectric constant

$$\epsilon_{eff} = 4\pi(p + s)\, C_{eff} = \epsilon \frac{p + s}{p + \epsilon s} \quad . \tag{6.2-11}$$

Using Eq. (6.2-7), we obtain

$$\epsilon_{eff} = \frac{\omega^2 - \omega_p^2}{\omega^2 - \omega_r^2} \quad , \tag{6.2-12}$$

where

$$\omega_r^2 = \frac{s}{p+s}\, \omega_p^2 \quad . \tag{6.2-13}$$

The sheath thickness $s$ is usually of order $5h$, where $h$ is the Debye length; for $p$ one should substitute the distance over which the rf field extends. It is clear from Eq. (6.2-12) that a resonance occurs at $\omega = \omega_r < \omega_p$, and that quite the contrary occurs at $\omega = \omega_p$: the impedance is maximum, and no rf current flows. The finite height and width of the resonance peak may be found by including an imaginary collision term in the denominator of Eq. (6.2-7); the result has been given by Mayer (15) and by Harp (16).

Fig. 6.6

The equivalent circuit of the system, as explained by Uramoto et al. ( 17 ) and by Levitskii and Shashurin ( 14 ), is shown in Fig. 6.6. The capacitances $C_p$ and $C_s$ represent the (leading) displacement currents that would flow even if the electrons were immobile; these correspond to the term "1" in Eq. (6.2-7). Because of the thinness of the sheath, we have $C_s > C_p$. The inductances $L_p$ and $L_s$ represent the (lagging) conduction currents of electrons and correspond to the second term of Eq. (6.2-7). $L_s$ is small and non-uniform and has been neglected in this treatment. The diode D represents the rectification of the conduction current in the sheath due to electron collection by the probe; currents in the plasma are not rectified unless the electrons oscillate with sufficient amplitude to reach the probe. This circuit gives the physical picture of the resonance probe phenomenon.

At low frequencies there is only an adiabatic change in the dc probe current, giving the flat portion at the left of the curves of Fig. 6.4. At a frequency $\omega = (L_p C_s)^{-\frac{1}{2}} = \omega_r$, $L_p$ is in series resonance with $C_s$, and the rf current to the probe is at a maximum. The rectified current is also maximum here, because the rf voltage between P and S, across the diode D, is maximum. This gives the resonance peak in Fig. 6.4. The height of the peak is limited by collisions in the plasma, represented by the resistance R. At a higher frequency $\omega = (L_p C_p)^{-\frac{1}{2}} = \omega_p$, $L_p$ is in parallel resonance with $C_p$, and the impedance of the circuit becomes large. The rf current to the probe is then at a minimum; the rectified current is also small because $C_s$ is a good conductor at this frequency, and little rf voltage appears across the diode D. Note that this frequency depends only

on $\omega_p$, whereas $\omega_r$ depends on the sheath thickness. At still higher frequencies the rf current increases again as the impedance of $C_p$ and $C_s$ diminish; the rectified current, however, continues to decrease as $L_s$ comes into play to limit the current through D — the inertia of the electrons limits the amplitude of their motion.

The main features of this model have been checked experimentally by Mayer ( 15 ) at plasma densities from $10^{10}$ to $10^{11}$ $cm^{-3}$. It was necessary to use a coaxial probe at the frequencies involved. Although the geometry was not planar, the measured value of $\epsilon_{eff}$ had a resonance and changed sign at $\omega = \omega_r < \omega_p$, in accordance with Eq. (6.2-12); and $\epsilon_{eff}$ went to zero at $\omega = \omega_p$, with $\omega_p$ determined from the saturation ion current. More precise measurements by Uramoto et al. ( 17 ) at densities around $10^6$ $cm^{-3}$ showed indeed that the rf and dc components peaked at the same frequency, and that the rf component had a minimum at a higher frequency, while the dc component decreased monotonically with frequency after the peak. These results are shown in Fig. 6.7. Measurements of phase shifts further confirmed the series resonance phenomenon. Unfortunately, no independent measurement of $\omega_p$ could be made. The variation of $\omega_r$ with sheath thickness $\underline{s}$ predicted by this model was observed in the experiment of Peter et al. ( 12 ) described previously.

Fig. 6.7

6.2.3 Detailed Computations

We now return to problem (I): the self-consistent calculation of the rf field distribution in the sheath and the plasma. This problem has been treated in detail both theoretically and experimentally in the beautiful work of Harp, Kino, and Pavkovich ( 18 ). In the calculations of Pavkovich and Kino ( 19 , 20 ), the collisionless, linearized, one-dimensional Boltzmann equation was integrated through a uniform plasma region with a Maxwellian electron distribution and an inhomogeneous sheath region in which the potential varies parabolically. Typical results for the rf field are shown in Fig. 6.8. Also shown in Fig. 6.8 are direct measurements of this field distribution, made by means of a probing electron beam by Harp and Kino ( 21 ). The agreement between theory and experiment can be considered excellent. As one would expect intuitively, the rf field is well shielded out by the sheath for $\omega \ll \omega_p$ but extends into the plasma for $\omega$ approaching or exceeding $\omega_p$.

Fig. 6.8

The work of Harp et al. removes any doubt about the magnitude of the "effective shielding length" in the heuristic theories of Ichikawa and Ikegami ( 11 ) and of Mayer ( 15 ). However, since the results can be expressed only in numerical form, the simplified models are still useful for obtaining a semi-quantitative grasp of the physical situation.

Harp ( 16 ) has applied the one-dimensional computation of Pavkovich to the more physically interesting case of a spherical probe of radius R by assuming that in the spherically symmetric case the fields should be multiplied by a factor $(R/r)^2$. Since the theory is a collisionless one, the only damping mechanism is Landau damping, which limits the Q of the resonance to about 10. For R less than about 2h, the resonance becomes very small. The resonant frequency can be approximated by Eq. (6.2-13), with $s = 5h$ and $p = R$. When neutral collisions are dominant, Eq. (6.2-13) must be used with a collision term. Harp ( 16 ) has checked the dielectric slab model by measuring the rf field near the probe by means of the electron beam technique. A peak was observed at $\omega = 0.6\,\omega_p$. This experiment clearly shows that resonance rectification is due to the large amplitude of the electric field when the admittance of the plasma-sheath system becomes large, in accordance with Fig. 6.6.

In all the above work, the actual mechanism of rectification, that is, problem (III) mentioned at the beginning of Sec. 6.2, has been neglected. This problem has been treated in more detail by Ichikawa ( 22, 23 ). In this work the transit time of the electrons across the sheath is taken into account by assuming that the electrons enter the sheath with random phases and are then accelerated by a sheath field with a dc component plus an rf component of magnitude $\delta V/L$. Although it is not clear what L is, this treatment correctly predicts that for very high frequencies the electron oscillation amplitude goes to zero, and $\langle j_e \rangle$ falls to the dc value. This behavior is in agreement with Fig. 6.4 but was not predicted in the original formula

(6.2-3), in which $\delta\langle j_e\rangle$ was defined as the increase over the low-frequency level $j_{eo} I_o(\delta\eta)$. The transit time also has the effect of diminishing the peak height. Ichikawa ( 24 ) has also considered the effects of nonlinear terms in the Fokker-Planck equation. The results of this rather elaborate theory, which also includes transit-time effects but neglects the sheath inhomogeneity, show that the peak height is considerably reduced by the nonlinear terms if $\delta\eta$ is larger than about 2 .

A theory which incorporates both the sheath effects and the transit-time effects has been given by Wimmel ( 13 ). This is a modification of the dielectric slab model in which the sheath boundary is taken to be the plane where the applied frequency is equal to the local plasma frequency, as found from the Child-Langmuir approximation, Eq. (2.2-5). Inside this sheath the rf potential is assumed to be equal to that on the probe, and outside the sheath the plasma is assumed to be homogeneous. The treatment of the exterior region resembles that of Ichikawa and Ikegami ( 11 ), except that the macroscopic fluid equations are used; hence Landau damping is neglected. Transit time is accounted for by assuming constant electron velocities in the sheath. After numerical computation, resonance probe characteristics are obtained which give the correct dependence on the probe bias $\eta_p$ .

Recently Uramoto et al. ( 25 ) have investigated the behavior of resonance probes in a weak magnetic field $\underline{B}$ . Their interesting data are consistent with the following picture. When $\underline{B}$ is parallel to the electric field $\underline{E}$ , no change in the resonance occurs other than that due to an increase in plasma density caused by the magnetic confinement. When $\underline{B}$ is perpendicular

to $\underline{E}$, no great change occurs for $\omega_c < \omega_p$, where $\omega_c$ is the electron cyclotron frequency. For $\omega_c > \omega_p$, however, the ordinary resonance peak disappears, since electrons can no longer follow the lines of $\underline{E}$; and a peak appears at $\omega_c$. Since the cyclotron peak appears only for $\omega > \omega_p$, when the rf field can penetrate into the plasma, the peak is attributed to plasma heating at cyclotron resonance; this conjecture has been corroborated by temperature measurements.

### 6.2.4 RF Transmission Between Probes

A technique closely related to the resonance probe is that of rf transmission between two probes. The only difference is that the probes need not be in actual contact with the plasma, since only the rf component of the current is measured. This technique was first employed by Yeung and Sayers (26), who transmitted a 300 Mc signal from one completely insulated probe to another across the diameter of the plasma. A resonance was observed as the plasma density was changed; this was interpreted as a resonance at $\omega = \omega_p$. That the resonance should occur at $\omega_r < \omega_p$ was pointed out by Levitskii and Shashurin (14), who gave the correct interpretation in terms of Fig. 6.6. Their data are shown in Fig. 6.9.

Fig. 6.9

A minimum appears at $\omega_p^2/\omega^2 = 1$, and a maximum at $\omega_p^2/\omega^2 = 5$, corresponding to the series resonance of $C_s$ and $L_p$ in Fig. 6.6. It is clear that if the probes are capacitively coupled to the plasma by, say, a glass wall,

the capacitance of the glass should be included in $C_s$. The second maximum in Fig. 6.9 was attributed to waves propagating along the surface of the plasma. The sharp minimum in Fig. 6.9 is independent of $C_s$ and gives a good measure of $n_e$; however, Uramoto et al. ( 17 ) point out that a minimum is not always easy to detect because of background noise.

Use of rf probes to measure electron density in the ionosphere has been made by Ikegami and Takayama ( 8 ), and by Haycock and Baker ( 27 ).

## 6.3 Ionic Frequencies: Pulsed Probes

### 6.3.1 Description of the Problem

We now wish to consider the response of a probe to a pulsed voltage. Since this response will be limited by the relatively slow motion of the ions, this is the problem of what happens when a relatively low frequency is superimposed on the probe voltage. The solution of this problem will give the maximum speed at which "dc" probe characteristics can be taken. One would expect intuitively that the sheath would change adiabatically at frequencies below that corresponding to the time it takes an ion to move across the sheath. Since in order of magnitude the ion velocity is the acoustic velocity $(kT_e/M)^{\frac{1}{2}}$ and the sheath thickness is the Debye length $[kT_e/(4\pi ne^2)]^{\frac{1}{2}}$, the critical frequency would be around the ion plasma frequency $\omega_{pi} = (4\pi ne^2/M)^{\frac{1}{2}}$.

This problem differs from that of the resonance probe in several important respects. First, of course, the ion motion must be considered. On the other hand, at these frequencies the electrons can be considered to react instantaneously to the electric field, and their inertia can be neglected. Second, at these low frequencies the electrons are always able to shield the oscillating potential from the plasma; hence there is no question of the penetration of the rf field into the plasma. Instead, the observed effects are caused by an oscillation in sheath thickness, an effect which was neglected in the theories of the resonance probe. Because of the good shielding, there will be only a weak coupling to waves in the plasma. (The excitation of ion waves by Wong et al. ( 28 ) by an electrostatic grid, therefore, is attributed instead to a modulation of the ion velocity distribution.) For simplicity, we shall be concerned with a plane probe, for which there is no change of sheath area as the sheath thickness changes. Clearly, then, there is no change in the dc component of probe current with frequency; the average current will always be given by the constant current entering the collisionless region. Finally, because one is perforce concerned with the ac component of probe current, the displacement current must be carefully taken into account explicitly.

In the collisionless case the fundamental equations are Poisson's equation,

$$\nabla^2 V = - 4\pi e (n_i - n_e) \quad , \qquad (6.3\text{-}1)$$

the equation of motion,

$$m_k (\partial \underset{\sim}{v}_k / \partial t + \underset{\sim}{v}_k \cdot \nabla \underset{\sim}{v}_k) = -e\nabla V , \qquad (6.3\text{-}2)$$

and the equations of continuity ,

$$\partial n_k / \partial t + \nabla \cdot (n_k \underset{\sim}{v}_k) = 0 , \qquad (6.3\text{-}3)$$

where $k = i, e$ . These are nine scalar equations in nine unknowns, to be solved with appropriate boundary conditions at the probe and at infinity. A general analysis of this system is not available, but fortunately this is a case where experimental results are available to lead the way. Recent investigations by Bills et al. ( 29 ) and by Oskam et al. ( 30 ) make clear what physically happens when a probe is pulsed. It turns out that the phenomenon is qualitatively different in different regions of the probe characteristic, and we shall consider these in turn.

### 6.3.2 Saturation Ion Current

Consider the special case of an infinite plane probe biased to collect saturation ion current. The electron current is then so small that we may assume that the electron distribution is always Maxwell-Boltzmann. For further simplicity, we shall assume that the ions are cold and stream into the collisionless region with a velocity given by the sheath criterion, Eq. (2.3-10). What one would expect to happen physically when the probe potential is suddenly changed from $V_1 < 0$ to $V_2 < V_1$ is illustrated in Fig. 6.10.

Fig. 6.10

In Fig. 6.10a is shown schematically the potential distribution in the sheath in the initial and final states. One can characterize the change loosely as a change in sheath thickness from $s_1$ to $s_2$. In Fig. 6.10b is shown the corresponding shift in the density distributions. The number of ions represented by the shaded region must be removed to form the new sheath, and therefore a transient ion current must flow to the probe. While the ion density is being adjusted, the potential will take an intermediate position such as that shown by the dashed curve in (a). Note that when the potential is pulsed back to $V_1$, the electron distribution moves to the left before the ions can move, and a region of negative space charge can exist near the sheath edge. Hence the potential curve can have an inflection point, as shown by the dotted curve in (a).

The transient current to the probe will be composed of a displacement current $j_d$ and an ion current $j_i$; we neglect the electron current. To be more specific, we integrate Poisson's equation over the usual pillbox containing the probe surface to obtain

$$E_p = 4\pi\sigma \ , \tag{6.3-4}$$

where $E_p$ is the value of the electric field at the probe surface and $\sigma$ is the surface charge on the probe. Taking the time derivative, denoted by a dot, and defining the total probe current $j_p$ to be positive when ions flow <u>from</u> the probe to the external circuit and the ion current $j_i$ to be positive when ions flow <u>to</u> the probe, we obtain

$$\dot{E}_p = 4\pi\dot{\sigma} = 4\pi e\,(j_i - j_p) \ , \tag{6.3-5}$$

$$4\pi e j_p = 4\pi e j_i - \dot{E}_p = 4\pi e\,(j_i + j_d) \ . \tag{6.3-6}$$

Thus the displacement current is given by the change of slope of the potential curve in Fig. 6.10a at $x = 0$.

Fig. 6.11

The response of the probe to a square pulse is illustrated in Fig. 6.11. The displacement current has a brief positive spike as $E_p$ abruptly jumps to the value given by curve (3) in Fig. 6.10a. In practice the height of this spike will be limited by the inductance in the circuit and the rise time of the voltage pulse. After the initial jump $E_p$ slowly relaxes to that given by curve (2) as the ions move to the new equilibrium distribution; this gives a small negative $j_d$. On the latter time scale the ion current is also collected by the probe; the total probe current therefore has the general behavior shown by the dotted curve in Fig. 6.11. In terms of the sheath capacitance $C_s$, the displacement current can be thought of as being composed of two parts:

$$ej_d = \dot{\sigma} = C_s \dot{V}_p + \dot{C}_s V_p \,. \qquad (6.3\text{-}7)$$

The first term corresponds to the fast initial spike, while the second term corresponds to the slow change in sheath capacitance as the sheath thickness changes from $s_1$ to $s_2$.

To compute $j_i$ and $j_d$, one must solve the time-dependent equations (6.3-1) to (6.3-3). It will be convenient to normalize distances to the Debye length, frequencies to the ion plasma frequency, and velocities to the sound velocity. Thus we introduce the dimensionless quantitites:

$$\eta = -eV/kT_e \quad , \qquad \nu = n_i/n_o$$

$$u = v_i/v_s \quad , \qquad v_s = (2kT_e/m_i)^{\frac{1}{2}}$$

$$\xi = x/h \quad , \qquad h = (kT_e/4\pi n_o e^2)^{\frac{1}{2}}$$

$$\tau = v_s t/h = \sqrt{2}\,\omega_{pi} t \tag{6.3-8}$$

$$\Omega = \omega/\sqrt{2}\,\omega_{pi}$$

$$-J = n_i v_i/n_o v_s$$

$$(') = \partial/\partial\xi \quad , \quad (\dot{}) = \partial/\partial\tau \quad .$$

With the electron distribution assumed to be Maxwellian, the fundamental equations (6.3-1) to (6.3-3) can be written one-dimensionally as follows:

$$\eta'' = \nu - e^{-\eta} \tag{6.3-9}$$

$$\tfrac{1}{2}\eta' = \dot{u} + uu' \tag{6.3-10}$$

$$\dot{\nu} + (\nu u)' = 0 \quad . \tag{6.3-11}$$

As it stands this nonlinear system is rather difficult to solve. To make further progress we shall assume that the oscillating potential on the probe is small compared to $kT_e$ and is of the form $\exp(-i\Omega\tau)$, so that the equations can be linearized. In equilibrium the time derivatives vanish, and we have

$$\eta_o'' = \nu_o - \exp(-\eta_o) \tag{6.3-12}$$

$$\tfrac{1}{2}\eta_o' = u_o u_o' \tag{6.3-13}$$

$$(\nu_o u_o)' = 0 \tag{6.3-14}$$

The Bohm problem is obtained by taking the approximate boundary conditions

$$\eta_o = \eta_p \quad \text{at} \quad \xi = 0$$

$$\eta_o = \eta_o' = 0 \quad \text{at} \quad \xi = \infty \tag{6.3-15}$$

$$\nu_o = 1, \quad u_o = -J_{oo} \quad \text{at} \quad \xi = \infty .$$

Integration of Eqs. (6.3-14) and (6.3-13) then yields

$$\nu_o u_o = -J_{oo} \tag{6.3-16}$$

and

$$u_o = -(\eta_o + J_{oo}^2)^{\frac{1}{2}} , \tag{6.3-17}$$

where we have taken the minus sign to be consistent with the direction of the positive x-axis in Fig. 6.10a. Eliminating $u_o$ and substituting for $\nu_o$ in Eq. (6.3-12), we obtain an equation for $\eta_o$ which can be integrated once explicitly to give the following:

$$\eta_o' = -\sqrt{2}\left\{2J_{oo}\left[(\eta_o + J_{oo}^2)^{\frac{1}{2}} - J_{oo}\right] + e^{-\eta_o} - 1\right\}^{\frac{1}{2}} \tag{6.3-18}$$

The condition that $\eta_o'$ be real for small $\eta_o$ gives the sheath criterion (2.3-10); thus

$$J_{oo}^2 \geq \tfrac{1}{2} . \tag{6.3-19}$$

We may take $J_{oo}^2 = \frac{1}{2}$ and integrate Eq. (6.3-18) numerically from the probe to infinity to obtain the zero-order potential distribution $\eta_o(\xi)$.

If we now set $\eta = \eta_o + \eta_1$, etc., and assume that all first-order quantities vary as $\exp(-i\Omega\tau)$, Eqs. (6.3-9) to (6.3-11) become, in first order,

$$\eta_1'' = \nu_1 + \eta_1 e^{-\eta_o} \tag{6.3-20}$$

$$\tfrac{1}{2}\eta_1' = -i\Omega u_1 + (u_o u_1)' \tag{6.3-21}$$

$$-i\Omega \nu_1 + (\nu_o u_1 + \nu_1 u_o)' = 0 . \tag{6.3-22}$$

By laboriously eliminating $u_1$ and $u_1'$ from the last two equations and their derivatives, and by inserting the resulting expression for $\nu_1$ into Eq. (6.3-20), one can obtain a complicated fourth-order equation for $\eta_1$ with complex coefficients which are functions of $\eta_o$ and the other zero-order quantities. This equation can be integrated numerically with the boundary conditions

$$\eta_1 = \delta\eta \text{ at } \xi = 0 , \quad \eta_1 = \eta_1' = \eta_1'' = 0 \text{ at } \xi = \infty \tag{6.3-23}$$

to give the complex function $\eta_1(\xi)$. The displacement current is then essentially $\eta_1'(0)$ and the ion current $J_1(0)$, where $-J_1 = \nu_o u_1 + \nu_1 u_o$. We have not deemed it worthwhile to make this tedious computation. Instead, we shall be content with some physical insights obtainable from an even more simplified model.

This is to use the Child-Langmuir approximation of neglecting the exponential term in Eq. (6.3-9) representing the electron density in the sheath. Since the asymptotic behavior of $\eta$ is ruined by this assumption, a sheath edge must be imposed at $\xi = \xi_s$. Furthermore, $u_o$ will be assumed to vanish at $\xi = \xi_s$, while the current $J_{oo}$ entering the sheath

remains finite; hence $\nu_o$ is infinite at $\xi_s$ (an integrable singularity). Note that in the plane case a natural definition of the sheath edge does not arise from the breakdown of the quasi-neutral solution, as it does in the spherical and cylindrical cases, because the quasi-neutral equation, which is essentially Eq. (6.3-18) with $\eta_o' = 0$, does not contain the coordinate $\xi$ explicitly. The zero-order equations (6.3-16), (6.3-17), and (6.3-12) now become

$$\nu_o u_o = -J_{oo} \tag{6.3-24}$$

$$u_o = -\eta_o^{\frac{1}{2}} \tag{6.3-25}$$

$$\eta_o'' = \nu_o = J_{oo}/\eta_o^{\frac{1}{2}} . \tag{6.3-26}$$

This can be integrated twice to obtain

$$\eta_o^{3/4} = \frac{3}{2} J_{oo}^{\frac{1}{2}} (\xi_s - \xi) , \tag{6.3-27}$$

where

$$\xi_s = \frac{2}{3} J_{oo}^{-\frac{1}{2}} \eta_p^{3/4} . \tag{6.3-28}$$

This is just the Child-Langmuir equation (2.2-5). The value of $J_{oo}$ is unspecified; from the sheath criterion we know it is approximately $1/\sqrt{2}$. If $\eta_p$ is varied slowly compared to the transit time of an ion, it is clear that the steady current $J_{oo}$ will flow to the probe, while $\xi_s$ merely shifts back and forth around the equilibrium position. If $\eta_p$ is varied very fast, it is clear that the ions cannot respond to the ac potential, and only the displacement current will be measured. In an intermediate frequency range, where $\Omega$ in Eqs. (6.3-21) and (6.3-22) is of the order of $u_o'$ and $\nu_o$ given above, there will be a phase shift between the ion motion and the probe potential; and an ac conduction current will be seen by the probe. We would expect a resonance for $\Omega \lesssim 1$.

Although the Child-Langmuir approximation is known to be accurate for the equilibrium solution, it is entirely too crude for the perturbation. For instance, if we neglect the exponential term in Eq. (6.3-20), Eqs. (6.3-20) and (6.3-22) give

$$J_1' = i\Omega \eta_1'' \quad . \tag{6.3-29}$$

At some new position $\xi_{s1}$ of the sheath edge, we require $\eta_1'$ to vanish. Since the probe potential is not felt beyond this point, only the current $J_{oo}$ is incident at $\xi_{s1}$; hence $J_1$ vanishes there. With this boundary condition, Eq. (6.3-29) can be integrated from 0 to $\xi_{s1}$ to give

$$J_1(0) = - i\Omega \eta_1'(0) \quad . \tag{6.3-30}$$

One can easily verify that this is just the negative of the displacement current, given by Eq. (6.3-6), at all frequencies. Hence the entire effect must come from the boundary, where the electron density is finite. It is just this region which is difficult to treat, since the boundary-layer methods used in Chapter 3 are no longer useful.

If one proceeds to neglect the electron density in Eq. (6.3-20), one can obtain a fairly simple equation for the oscillating potential in the interior of the sheath. Equation (6.3-22) is integrated as above, and $u_1$ is eliminated using Eq. (6.3-21). When the zero-order quantities given by Eqs. (6.3-24 to 28) are substituted into the resulting third-order equation for $\eta_1$, one notes that a scaling of $\xi$ with $\Omega$ is possible. Thus one introduces

$$\zeta = \left(\frac{2}{3}\right)^2 J_{oo}^{-1} \Omega^3 (\xi_s - \xi) \qquad (6.3\text{-}31)$$

to obtain the equation

$$\zeta^{2/3} \eta_1''' + 2(\zeta^{-1/3} - i)\eta_1'' - [\zeta^{-1}(\zeta^{1/3} + \tfrac{4}{3} i) - \tfrac{2}{9}\zeta^{-4/3}]\eta_1' = 0 , \qquad (6.3\text{-}32)$$

where the primes now denote $d/d\zeta$. This equation does not contain $\Omega$; however, $\Omega$ determines the position of the sheath edge $\zeta_s$. The boundary condition at $\zeta = 0$ is $\eta_1 = \delta\eta$, but the boundary condition at $\zeta_s$ is not easily formulated, for, among other things, the zero-order density is discontinuous at $\zeta_s$.

The Child-Langmuir solution is useful nonetheless for estimating the relative importance of the displacement and conduction currents. The total charge of ions that flows transiently to the probe when it is pulsed from $V_1$ to $V_2$ (Fig. 6.10) is given by

$$q_i = en_o h \Delta \left( \int_o^{\xi_s} \nu_o \, d\xi \right) . \qquad (6.3\text{-}33)$$

Substituting for $\nu_o$ from Eqs. (6.3-26) and (6.3-27) and integrating, we obtain

$$q_i = 2e n_o h J_{oo}^{\frac{1}{2}} \Delta(\eta_p^{\frac{1}{4}}) . \qquad (6.3\text{-}34)$$

The integral of the displacement current $ej_d$ over time is found from Eq. (6.3-6) to be

$$q_d = -\frac{1}{4\pi} \frac{kT_e}{eh} \Delta\eta'(0) . \qquad (6.3\text{-}35)$$

Using the value of $\eta'$ from the differential of Eq. (6.3-27), we find that $q_d = q_i$. Thus $j_d$ and $j_i$ differ only because the charges $q_d$ and $q_i$ flow at different rates. In the experiment of Kamke and Rose discussed in Sec. 4.5.4 it is not clear whether $q_i$ or $q_i + q_d$ was actually being measured.

Experimentally, Oskam et al.[30] have observed a fast pulse of $j_d$ as a negative probe was given a square pulse. The ion current was apparently too small to be observed. A carefully shielded probe had to be used to eliminate the capacitance between the probe lead and the plasma. Phase measurements at different frequencies showed only the effect of the sheath capacitance when the probe was in the saturation ion region. No measurements of the "resonance probe" type, showing a peak of $j_i$ near or below $\omega_{pi}$, are available; nor is a solution of Eqs. (6.3-20 to 22) with proper boundary conditions.

6.3.3 Saturation Electron Current

Consider now the case of a probe biased positively to draw saturation electron current. The probe current, according to Eq. (3.1-1), will be given approximately by $I_e = A_s j_r$, where $A_s$ is the area of the sheath surface and $j_r$ is the random current. The ions will have a Maxwell distribution, and the electron density and the potential will again be given approximately by the Child-Langmuir law. When the probe is pulsed further positive, these distributions are shown in the initial and final states by the solid curves of Fig. 3.10, with the subscripts i and e interchanged and -V replaced by V. The ions, being massive, take time to move out of the space between $s_1$ and $s_2$. Before the ions have had a chance to move, the electron distribution must adjust to the new probe potential without the benefit of a change in the ion distribution. A little thought will reveal that this causes some difficulty in the strictly plane case. Furthermore, since the entire random current is collected anyway, and $A_s$ cannot increase in the plane case, there can be no change in $j_e$, the current of electrons being conserved even in the transient state because of their negligible inertia. To explain the observed results we must go to finite geometry and the case of spherical or cylindrical probes.

Fig. 6.12

In Fig. 6.12 the solid curves represent the initial distributions about a spherical or cylindrical probe. When the probe is pulsed from $V_1$ to $V_2$, the electron density for $r > s_1$ cannot be below $n_i$; otherwise, the electric field would be in a direction to drive the ions toward the probe. If the geometry were planar, $n_e$ could also not be larger than $n_i$, since this would require deceleration of electrons, again by field in the wrong direction. However, in finite geometry $n_e$ can be larger than $n_i$ even when the electrons are accelerated, because of geometrical compression. Thus the density and potential distributions in the transient state can be somewhat as depicted by the dashed curves in Fig. 6.12. The transient sheath radius $s_t$ is obviously greater than $s_2$, because of the presence of ions interior to $s_2$; in fact, $s_t$ must be comparable to the probe radius in order for geometrical effects to be felt. Therefore the transient value of $j_e$ is larger than the final value, and an overshoot in $j_e$, as shown in Fig. 6.13, would be expected. Its duration would be of order $\omega_{pi}^{-1}$, the time it takes the ions to move from $s_1$ to $s_2$. The reader can easily convince himself that the transient sheath radius upon pulsing back to $V_1$ cannot be smaller than $s_1$, and therefore no overshoot on the downward side is expected.

Fig. 6.13

A current response like that in Fig. 6.13 has been observed by Bills et al. ( 29 ) with a cylindrical probe in a low-pressure mercury discharge with densities of order $10^{11}$ $cm^{-3}$. Since the overshoot does not appear unless there is an electron sheath around the probe, the appearance of the overshoot as the probe potential is increased is a good indication of the space potential. The overshoot has also been observed by Bol and Fujita ( 31 ) in a strong magnetic field. Here the sheath must grow at least partially across the magnetic field to give the increase in current. The overshoot was observed for heavy gases but not for H and He. Because the plasma density was above $10^{13}$ $cm^{-3}$, the probe response time was comparatively fast, and an essentially dc probe characteristic could be obtained in a few tenths of microseconds.

To work out a theory for this phenomenon would obviously be more difficult than for the negative pulsed probe, since both the $n_i$ and $n_e$ terms in Eq. (6.3-1) are important, and the full set of equations (6.3-1) to (6.3-3) must be used. Furthermore, since the electrons are normally hotter than the ions, for accuracy it would be necessary to integrate over the distribution of electron velocities. We can, however, estimate the relative importance of the displacement current. Since the Child-Langmuir potential distribution is independent of mass, and $j_d$ is specified by $\eta'(0)$, the total displacement charge $Q_d$ can be found from Eq. (6.3-34):

$$Q_d \approx \frac{1}{2} e n_o A_p h \eta_p^{-3/4} , \qquad (6.3\text{-}36)$$

where $A_p$ is the probe area. The total charge $Q_e$ contained in the overshoot in $j_e$ is given by the random electron current times the excess sheath area $\Delta A_s$ during the overshoot times the duration of the overshoot. If $\Delta A_s \approx A_p$ we have approximately

$$Q_e \approx e A_p j_r/\omega_{pi} = e n_o A_p h (M/2\pi m)^{\frac{1}{2}} \quad . \qquad (6.3\text{-}37)$$

Therefore $q_d/q_e$ is of order $(m/M)^{\frac{1}{2}}$, and the displacement current is negligible for a pulsed positive probe.

6.3.4 Effect of Collisions

In contrast to the results of Bills et al. (29), Oskam et al. (30) did not observe an overshoot in the current to a positive pulsed probe; instead the electron current rose slowly to the new equilibrium value. The difference may be caused by collisions. The experiment of Bills et al. was done in a low-pressure ($10^{-3}$ torr), high-current (1 amp) discharge, while that of Oskam et al. was performed in a high-pressure (1 torr), low-current (1 ma) discharge. When a positive probe is pulsed at high pressures, the current cannot rise fast because it is limited by collisions in the quasi-neutral region. Instead, the current lags until ions in the entire perturbed quasi-neutral region move to set up the gradients necessary to supply the increased electron current by diffusion. From this picture, one would expect that the time it takes to reach equilibrium would be inversely proportional to the ion mobility $\mu_i$; indeed, by varying the ion mass and the neutral density, Oskam et al. (30) verified that the response time had the proper dependence.

In the continuum limit, an estimate of the response time can easily be made, since the ion velocity is now a linear function of the potential:

$$v_i = -\mu_i \nabla V \quad . \qquad (6.3\text{-}38)$$

Combining this with Poisson's equation (6.3-1) and the ion equation of motion (6.3-3), we obtain the equation

$$D n_i/D t + 4\pi \mu_i e n_i(n_i - n_e) = 0 , \qquad (6.3\text{-}39)$$

in which $D = \partial/\partial t + \underline{v} \cdot \nabla$ is the derivative in the rest frame of the ions. The electron density $n_e$ is a rapid function of time; but if we consider only highly negative probes, $n_e$ can be neglected. The solution is then

$$\frac{1}{n_i} - \frac{1}{n_o} = 4\pi \mu_i e t . \qquad (6.3\text{-}40)$$

Thus in the continuum limit the response time of an ion sheath is indeed proportional to $\mu_i^{-1}$, at least in the ion frame of reference.

### 6.3.5 The Transition Region

When a probe biased in the transition region is pulsed, the change in electron conduction current is usually so large that it masks both the displacement current and the ion current due to a change in sheath thickness. Therefore, in a collisionless plasma a probe behaves as predicted by the dc theory (Secs. 3.2 and 6.1) up to frequencies near $\omega_{pe}$, where the theory of the resonance probe takes over. This has been verified by Bills et al. (29) and by the various authors investigating resonance probes. When the plasma is collision-dominated, however, an increase in electron current cannot take place until the proper gradients are set up in the diffusion region to supply this current. Consequently, Oskam et al. (30) report a long delay before a positively-pulsed probe in the transition region reaches equilibrium. When the

probe is given a negative pulse, however, the long delay does not appear, because the electron current can easily arrest itself by building up a negative space charge cloud.

### 6.3.6 Experimental Observations

In the work of Bills et al. ( 29 ), a 2 μsec square pulse was put on a probe in an essentially collisionless plasma with $n \cong 10^{11}$ cm$^{-3}$. The time for a probe in the saturation electron region to reach equilibrium was about 0.5 μsec. In the saturation ion region only the fast displacement current was observable. Because the transient ion current is so small, probes collecting ions have an apparently better frequency response than probes collecting electrons, contrary to one's first inclination. In the transition region the response time was below $10^{-8}$ sec, as expected. Probe characteristics taken with the pulsed probe yielded values of $kT_e$ and $n$ 10% higher than with dc methods; no explanation could be given. From these data it is clear that a "dc" probe characteristic cannot be taken with a sawtooth voltage in less than several microseconds.

The extensive investigations of Oskam et al. ( 30 ) were carried out at higher pressures, where collisions were important. A number of methods were used, including square pulses and Lissajous figures obtained with sine waves. In the saturation electron region the delay in reaching equilibrium was of order 1 μsec. In the saturation ion region the displacement current spike lasted about 0.4 μsec. In the transition region the delay for a positive-going probe was as long as 10 μsec. If $n$ was increased, the delays were

decreased and the displacement current increased, as one would expect from the decrease in Debye length. Comparison of probe characteristics taken by the dc and pulsed methods showed the largest discrepancy near the space potential, where the measured delays were greatest.

The low-frequency limit of the theory of Sec. 6.3.2 was investigated by Butler and Kino ( 9 ). In this experiment both square waves and sine waves were capacitively coupled to a ring on the inner wall of the discharge tube. The frequencies were so low that ion inertia could be neglected, and the sheath could be described by the Child-Langmuir approximation at all times. The displacement current was calculated from the shift in the position of the sheath edge, which amounts to the same thing as Eq. (6.3-35), and to this was added a larger ion current term due to the change in sheath area. This was essentially a dc ion current, unrelated to that discussed is Sec. 6.3.2. The calculated time response of the voltage on the ring agreed extremely well with experiment in spite of the fact that the plane sheath equation was used when the lack of saturation of ion current showed that the sheath was not planar. The reason is that the major part of the observed effect was the change in $j_i$, which was measured from the dc probe characteristic; thus the only quantity that was calculated was the small correction due to the displacement current.

Pulsed probes have also been used by Waymouth ( 32 ) ; the pulse length was 10 μsec, long enough to achieve equilibrium. The work by Kamke and Rose ( 33 ) on ion current was discussed in Sec. 4. 5. 4. In addition to these works, investigations in time-varying plasmas by Koch ( 34 ), Beck ( 35 ), Barnes ( 36 ), and Ledrus ( 37 ) have some bearing on this problem, at least in regard to circuitry and the comparison of dc and pulsed probe characteristics. Additional references can be found in Sec. 8. 1. on probe contamination.

## 6.4 Measurement of Random Fluctuations

### 6.4.1 Introduction

The use of electrostatic probes to detect plasma waves is commonplace. For instance, ion acoustic waves have been detected by Alexeff and Neidigh (38), longitudinal electron waves by Etievant and Perulli (39), and ion cyclotron waves by Motley and D'Angelo (40). We wish to consider here the measurement of random fluctuations, or low-frequency noise, in plasmas. Such fluctuations, in both density and potential, are often encountered in discharges which are sufficiently highly ionized that collisions between ions and neutrals do not play an important role in damping. An example of a continuous spectrum of such oscillations in a strong magnetic field is shown in Fig. 6.14. Very similar spectra are observed in entirely different types of discharges in magnetic fields; moreover, continuous spectra are also observed in the absence of a magnetic field. Since such fluctuations are thought to be connected with anomalously fast transport of plasma across magnetic fields, it is worthwile to try to understand their detailed statistical properties. For such studies Langmuir probes are the most suitable diagnostic tool because of their fine spatial resolution. Note that the spectrum of Fig. 6.14 cuts off well before the ion cyclotron or plasma frequency, so that transient effects need not be considered in using probes to measure fluctuations in $V_s$ and $n$ by observing the fluctuations in $V_f$ and $I_i$, respectively.

Fig. 6.14

The use of correlation techniques in studying turbulence in hydrodynamics is a well known procedure (41). In wind-tunnels, for instance, the statistically varying quantities are the velocity components of the gas. In a plasma the nature of the turbulence is not the same, and the quantities of interest are rather the local density and electric field or potential. The use of correlation techniques in dense plasmas was suggested by Spitzer (42); the first measurements were apparently made by Batten, Smith, and Early (43) in a cold-cathode reflex discharge. Subsequently, Crawford (44, 45) has measured the frequency spectrum of fluctuations in mercury discharges, with and without magnetic fields; Rusbridge et al. (46) have studied the fluctuating electric field in high-current toroidal discharges by means of double probes; Chen et al. (47, 48) have studied both the spectrum and the correlation function of oscillations in reflex arcs; and Rothman et al. (49) have measured the spectrum of density fluctuations in a weakly-ionized aerodynamic jet. The most extensive use of correlation techniques in plasmas, however, has been made in a dc stellarator (50) by Bol (51), whose approach we follow here.

### 6.4.2 Theory of Correlations

We wish here to outline, with no attempt at rigor, the general principles involved in the measurement of correlations. Consider a fluctuating quantity of interest $V(x,t)$ with zero average; this could be, for instance, the local plasma potential or the local density. Let $V$ be defined in a time interval $T$, long compared with the oscillation period involved; then the time behavior of $V$ at a given position can be described by a Fourier analysis in time:

$$V(t) = \sum_{-\infty}^{\infty} a_n e^{i\omega_n t} \quad , \tag{6.4-1}$$

where

$$\omega_n = 2\pi n/T \quad , \tag{6.4-2}$$

and

$$a_n = \frac{1}{T}\int_0^T V(t') e^{-i\omega_n t'} \, dt' \quad . \tag{6.4-3}$$

The nth Fourier component is then given by

$$V_n = a_n e^{i\omega_n t} + a_{-n} e^{-i\omega_n t} \quad , \tag{6.4-4}$$

and the power spectrum $P(\omega_n)$ is defined by

$$P(\omega_n) = \langle V_n^2 \rangle = \langle 2 a_n a_{-n} \rangle \quad . \tag{6.4-5}$$

The average $\langle \quad \rangle$ indicated above is to be taken over an ensemble of systems, which could be, for instance, separate pulses or parts of pulses of a repetitive discharge. Since we shall consider systems which are statistically uniform in time, the ensemble average can be regarded as a time average; and the second bracket $\langle \quad \rangle$ in Eq. (6.4-5) may be removed, the Fourier amplitudes $a_n$ being, of course, independent of time.

The autocorrelation function $R(\tau)$, or autocovariance, is defined as

$$R(\tau) = \langle V(t)\, V(t+\tau) \rangle \quad . \tag{6.4-6}$$

Again, statistical uniformity in time means that a time average may be taken

in Eq. (6.4-6), and $R(\tau)$ is independent of time. Inserting Eq. (6.4-1) making use of the orthogonality properties of the exponential, we obtain, with Eq. (6.4-5),

$$R(\tau) = \sum_{n=-\infty}^{\infty} a_n a_{-n} e^{i\omega_n \tau} = \sum_{n=1}^{\infty} \tfrac{1}{2} P(\omega_n)(e^{i\omega_n \tau} + e^{-i\omega_n \tau}) , \qquad (6.4\text{-}7)$$

since $P(\omega_n)$ is symmetric and $\omega_n$ is antisymmetric in $n$.

We thus have

$$R(\tau) = \sum_{1}^{\infty} P(\omega_n) \cos \omega_n \tau \quad . \qquad (6.4\text{-}8)$$

In the limit $T \to \infty$, the sum goes into an integral, and we recover the Wiener-Khinchine theorem, well known in the theory of communications ( 52 ). $R(\tau)$ and $P(\omega_n)$ are clearly Fourier transforms of each other, and the same information is contained in either $R(\tau)$ or $P(\omega_n)$.

We can make a similar analysis of the spatial dependence of $V(x,t)$ if it is statistically uniform over a region of space of dimensions $L$ much larger than the relevant wavelengths. Considering only one spatial dimension for brevity, we may decompose $V(x,t)$ into partial waves and define a "mode spectrum" $P(k_m, \omega_n)$ as follows:

$$V(x,t) = \sum_{-\infty}^{\infty} \sum_{-\infty}^{\infty} a_{mn} e^{i(k_m x - \omega_n t)} \qquad (6.4\text{-}9)$$

$$P(k_m, \omega_n) = \langle V_{mn}^2 \rangle = 2 \langle a_{mn} a_{-m-n} \rangle , \qquad (6.4\text{-}10)$$

where $k_m = 2\pi m/L$. The cross-correlation function $R(\xi, \tau)$ is defined as

$$R(\xi, \tau) = \langle V(x,t)\, V(x+\xi, t+\tau) \rangle \quad , \tag{6.4-11}$$

in which the ensemble average may be taken as an average over space and time if the turbulance is homogeneous. Inserting the expression (6.4-9) for $V$ and performing the averaging as before, we obtain, with the use of Eq. (6.4-10),

$$R(\xi, \tau) = \sum_{-\infty}^{\infty} \sum_{-\infty}^{\infty} \tfrac{1}{2} P(k_m, \omega_n)\, e^{i(k_m \xi - \omega_n \tau)} \quad . \tag{6.4-12}$$

Note that $P(k_m, \omega_n)$ is equal to $P(k_{-m}, \omega_{-n})$ but not necessarily equal to $P(k_{-m}, \omega_n)$. For positive values of $k$ and $\omega$, we can break the summand of (6.4-12) into four terms and obtain

$$R(\xi, \tau) = \sum_{1}^{\infty} \sum_{1}^{\infty} \left[ P(k_m, \omega_n) \cos(k_m \xi - \omega_n \tau) + P(k_{-m}, \omega_n) \cos(k_m \xi + \omega_n \tau) \right] . \tag{6.4-13}$$

In the limit $T \to \infty$, $L \to \infty$, this turns into a double integral over $dk$ and $d\omega$. The two terms in the summand obviously correspond to waves with the same $|\omega|$ and $|k|$ propagating in opposite directions. A normalized correlation function, or correlation coefficient, $\hat{R}(\xi, \tau)$ can be defined as

$$\hat{R}(\xi, \tau) = \frac{R(\xi, \tau)}{R(0,0)} = \frac{\langle V(x,t)\, V(x+\xi, t+\tau) \rangle}{\langle V^2(x,t) \rangle} \quad . \tag{6.4-14}$$

Even when the turbulence is homogeneous, the actual signals $V_1$ and $V_2$ from two probes may differ in rms magnitude because of differences in probe area or gain; in such a case the correlation coefficient is defined as

$$\hat{R}(\xi, \tau) = \langle V_1 V_2 \rangle / [\langle V_1^2 \rangle \langle V_2^2 \rangle]^{\frac{1}{2}} \quad , \tag{6.4-15}$$

The problem at hand is to determine the mode spectrum $P(k,\omega)$ of the turbulence. If the fluctuations are truly random, one would expect $P(k,\omega)$ to fill the $(\omega,k)$ plane uniformly. If, on the other hand, the continuous spectrum of Fig. 6.14 were due to a superposition of waves with a continuous range of $k$ but with a definite dispersion relation between $\omega$ and $k$, $P(k,\omega)$ would consist of narrow bands in the $(\omega,k)$ plane. A convenient way to measure $P(k,\omega)$ is to measure $\hat{R}(\xi,\tau)$ by means of two probes spaced $\xi$ cm apart, whose signals suffer a relative delay of $\tau$ sec. In fact, a great deal can be learned by setting $\tau = 0$ and fixing $\omega$ by passing the signals through a filter. We shall give simple examples of how $\hat{R}(\xi,0)$ might behave.

With $\omega_n$ fixed and $\tau = 0$, Eqs. (6.4-13) and (6.4-14) become, in integral form,

$$\hat{R}(\xi,0) = \int_0^\infty [P(k,\omega) + P(-k,\omega)] \cos k\xi \, dk \Big/ \int_0^\infty [P(k,\omega) + P(-k,\omega)] \, dk \quad . \qquad (6.4\text{-}16)$$

If the dispersion relation $k(\omega)$ allows only one value of $k$ for each value of $\omega$, we would observe a single wave at the given value of $\omega$. The correlation coefficient as a function of probe separation is then a simple cosine:

$$\hat{R}(\xi,0) = \cos k_\omega \xi \quad . \qquad (6.4\text{-}17)$$

By measuring the intercepts at $\hat{R} = 0$ for various $\omega$, one can obtain the dispersion relation $k(\omega)$. If, on the other hand, all values of $k$ between 0 and $K$ are equally probable for a given $\omega$, we may set $P = 1$ in Eq. (6.4-16) and obtain

$$\hat{R}(\xi, 0) = K^{-1} \int_0^K \cos k\xi \, dk = (K\xi)^{-1} \sin K\xi \, . \qquad (6.4\text{-}18)$$

This the transform of a band of white noise and is shown in Fig. 6.15.

Fig. 6.15

If $P(k, \omega)$ is a Gaussian peaked around $k_\omega$ with a half-width $\Delta k$, its transform is also a Gaussian. Putting

$$P(k, \omega) = A \, e^{-(k - k_\omega)^2/(2\Delta k)^2} \qquad (6.4\text{-}19)$$

into Eq. (6.4-16), one finds

$$\hat{R}(\xi, 0) = \cos k_\omega \xi \; e^{-(\Delta k)^2 \xi^2} \, . \qquad (6.4\text{-}20)$$

This is shown in Fig. 6.15 for two values of $\Delta k$. For a large spread $\Delta k$, $\hat{R}$ falls monotonically with a "correlation length" $(\Delta k)^{-1}$. For small spreads $\Delta k$, $\hat{R}$ is a damped cosine wave, whose intercepts give the value of $k_\omega$ and whose envelope gives an idea of the correlation distance. Finally, if for each $\omega$ there can be only one value of $k$ but a range of $k$ exists because of the finite width of the filter characteristic, then $P(k, \omega)$ might take the form

$$P(k, \omega) = A[1 + (2/\Delta k)^2 (k - k_\omega)^2]^{-1} \, . \qquad (6.4\text{-}21)$$

for $\Delta k \ll k_\omega$, one finds that $\hat{R}(\xi, 0)$ is an exponentially damped cosine:

$$\hat{R}(\xi, 0) = \cos k_\omega \xi \; e^{-\xi \Delta k/2} \, . \qquad (6.4\text{-}22)$$

Suppose now that for a given $\omega$ the magnitude of $k$ is fixed by the dispersion relation but that waves in opposite directions can exist simultaneously. From Eq. (6.4-16) we see that each wave would have the same value of $\hat{R}(\xi, 0)$ given by Eq. (6.4-17). To measure the standing wave ratio, we must introduce a delay $\tau$. Let us denote $P(k, \omega)$ by $P_+$ and $P(-k, \omega)$ by $P_-$. Then if we have a propagating wave such that $P_+ = 1$, $P_- = 0$, the correlation coefficient is given by

$$\hat{R}(\xi, \tau) = \cos(k_\omega \xi - \omega\tau) . \qquad (6.4\text{-}23)$$

From this it is clear that by varying $\tau$ one can always bring the value of $\hat{R}$ up to unity at any $\xi$. On the other hand, if $P_+ = P_- = 1$, so that there is a standing wave, the correlation coefficient is

$$\hat{R}(\xi, \tau) = \cos k_\omega \xi \cos \omega\tau . \qquad (6.4\text{-}24)$$

By varying $\tau$ one can only diminish $|\hat{R}|$ below the value for $\tau = 0$. Obviously, all points in a standing wave pattern already vibrate in phase, and a phase change can only decrease the correlation. Similarly, if $P_{\pm}$ has the Gaussian form $\exp[-(k \pm k_\omega)^2/(2\Delta k)^2]$, it can easily be verified that Eqs. (6.4-23) and (6.4-24) must merely be multiplied by $\exp[-(\Delta k)^2 \xi^2]$. Therefore, for a damped cosine changing the delay $\tau$ can bring $\hat{R}$ up to the envelope of the $\tau = 0$ curve if the waves are unidirectional; but it can only decrease $\hat{R}$ if there are standing waves. The effect of introducing $\tau$ is illustrated in Fig. 6.16.

Fig. 6.16

Sometimes for experimental reasons it is not possible to measure $\hat{R}(\xi, 0)$ beyond the first zero. Whether this zero corresponds to a true loss of coherence or merely to the first zero of a damped cosine can be resolved by introducing a delay $\tau$ of order $\pi/2\omega$. This would raise $\hat{R}$ to the amplitude of the envelope in the case of a damped cosine but would do nothing if the signals are uncorrelated, or if there is a standing wave pattern. To distinguish the latter two possibilities one can check whether or not the individual signal amplitudes vary with position.

The results obtained above are valid if the sampling time is infinitely long. Clearly, if the length of the samples is comparable to the period of the lowest frequency measured, a correction must be made to the apparent value of $\hat{R}$. Less obvious is the effect of the bandwidth $\Delta f$ of the frequency selector. To get a meaningful time average, the sample length must be long compared with $(\Delta f)^{-1}$; therefore, a weakly damped cosine for $\hat{R}(\xi)$ can be obtained only with very narrow bandwidths and very long samples.

6.4.3 Experimental Details

The correlation coefficient $\hat{R}(\xi, \tau)$ can be measured conveniently by taking the average mean squares of the sum and difference of the two probe signals $V_1$ and $V_2$. Let

$$P = \frac{\langle (V_1 - V_2)^2 \rangle}{\langle (V_1 + V_2)^2 \rangle} \quad \text{and} \quad Q = \frac{\langle V_1^2 \rangle}{\langle V_2^2 \rangle} \,. \qquad (6.4\text{-}25)$$

The correlation coefficient of Eq. (6.4-15) can then be written

$$\hat{R} = \frac{1 - P}{1 + P} \quad \frac{\Omega^{\frac{1}{2}} + \Omega^{-\frac{1}{2}}}{2} \tag{6.4-26}$$

If the gains are adjusted so that $V_1$ and $V_2$ are approximately equal in magnitude, the effect of the $\Omega$ terms in Eq. (6.4-26) is slight. $\hat{R}$ can then be computed readily from $P$; or one can use the graph of Fig. 6.17.

Fig. 6.17

Fig. 6.18

To measure $P$, Bol (51) uses the circuit of Fig. 6.18. It is possible to make correlation measurements of space potential by making $V_1$ and $V_2$ the floating potentials of two probes. In this case the source impedance is high, and good frequency response is not always easy to obtain. One can also make correlations of the plasma density by making $V_1$ and $V_2$ the voltages across current-measuring resistors of probes biased to draw saturation ion current. This is the situation depicted in Fig. 6.18. After passing through broad filters to remove noise outside the frequencies of interest and through a variable delay line which introduces $\tau$, the signals are fed to the inputs of a differential amplifier, which can be the preamplifier of an oscilloscope. By inverting the polarity of one signal, the output can be made $V_1 + V_2$ or $V_1 - V_2$. This passes through an accurate attenuator and then goes to a communications receiver to select a frequency $\omega$. It makes no difference

whether the frequency analysis is performed before or after the signals are added; therefore, only one receiver is required. The output of the if strip is then power amplified to drive a thermocouple, which is a frequency insensitive squaring device. The galvanometer reading is then a measure of $\langle (V_1 \pm V_2)^2 \rangle$. This reading is kept constant by the calibrated attenuator; the attenuator readings for the two positions of the polarity switch then give the value of $P$.

Fig. 6.19

Typical results obtained in this manner by Bol ( 51 ) are shown in Fig. 6.19. Since the perturbations were found to propagate primarily in the azimuthal direction, $\hat{R}$ was measured as a function of the probe separation $\Delta\theta$. It is seen that $\hat{R}$ is in the form of a damped cosine, from which $k(\omega)$ and the correlation distance could be obtained. The open circles in Fig. 6.19 are measures of the envelope of $\hat{R}(\Delta\theta)$ obtained by dividing $\hat{R}$ by $\cos k_\omega \Delta\theta$, with $k_\omega$ found from the intercepts at $\hat{R} = 0$ [c.f. Eq. (6.4-22)]. The maximum value of $\hat{R}(\Delta\theta, \tau)$ obtained by varying $\tau$ is indicated by the horizontal bars; since this falls on the envelope, the waves are unidirectional. From these curves it is seen that wavelength $\lambda$ decreases with increasing $\omega$, but not linearly. The waves apparently are carried with the macroscopic rotation of the plasma column but also have a velocity relative to the column.

Fig. 6.20

In Fig. 6.20 are shown data taken by Chen and Cooper ( 48 ) on correlation coefficients along the magnetic field $B$. Although the discharge

was considerably different from that used by Bol, the nature of the turbulence at high magnetic fields was very similar. Since the correlation function was a strong function of probe separation across $B$, to measure the longitudinal correlation it was necessary to align the probes accurately along $B$ by means of an electron beam. From these data it is seen that at high fields the oscillations are essentially in phase all along the plasma column. At higher frequencies than those shown, $\hat{R}(\xi)$ falls monotonically to zero, indicating a large spread in $k_z$ for each value of $\omega$. This is what would be expected from drift instabilities, for which $\omega$ is determined primarily by $k_\perp$ rather than $k_z$. These data render unlikely the hypothesis that the turbulence arises from Alfvén waves or ion acoustic waves.

From the point of view of anomalous diffusion, it would be desirable to measure the correlation in electric field $E$ directly by means of two pairs of probes, or, even better, the correlation between $E$ and density $n$ by means of two floating probes and a negatively-biased probe. However, because the presence of so many probes tends to disturb the plasma, this has not yet been achieved.

## REFERENCES


1. A. Garschadden and K.G. Emeleus, Proc. Phys. Soc. 79, 535 (1962).
2. F.W. Crawford, J. Appl. Phys. 34, 1897 (1963).
3. A. Boschi and F. Magistrelli, Nuovo Cimento 29, 487 (1963).
4. M. Sugawara and Y. Hatta, Inst. of Plasma Physics (Nagoya Univ., Japan) Research Report IPPJ-4 (1963).
5. S. Kojima, K. Takayama, and A. Shimauchi, J. Phys. Soc. (Japan) 8, 55 (1953).
6. R.B. Cairns, Proc. Phys. Soc. 82, 243 (1963).
7. F.F. Chen, Princeton Plasma Physics Laboratory Report MATT-62 (1961). (to be published in Rev. Sci. Instr.).
8. H. Ikegami and K. Takayama, Institute of Plasma Physics (Nagoya) Report IPPJ-10 (1963).
9. H.S. Butler and G.S. Kino, Phys. Fluids 6, 1346 (1963).
10. K. Takayama, H. Ikegami, and S. Miyasaki, Phys. Rev. Letters 5, 238 (1960).
11. Y.H. Ichikawa and H. Ikegami, Prog. Theor. Phys. (Japan) 28, 315 (1962).
12. G. Peter, G. Muller, and H.H. Rabben, Proceedings, Sixth Int'l Conf. on Ionization Phenomena in Gases, Paris, 1963, IV, p. 147. CIPIG, Orsay (Seine-et-Oise), France, 1964.
13. H.K. Wimmel, Inst. f. Plasma physik (Garching) Report IPP/6/11 (1963).

14. S. M. Levitskii and I. P. Shashurin, Sov. Phys. - Tech. Phys. 8, 319 (1963).

15. H. M. Mayer, Proceedings of the Sixth Int'l Conf. on Ionization Phenomena in Gases, Paris, 1963, IV, p. 129. CIPIG, Orsay (Seine-et-Oise), France, 1964.

16. R. S. Harp, Appl. Phys. Letters (1964).

17. J. Uramoto, J. Fujita, H. Ikegami, and K. Takayama, Institute of Plasma Physics (Nagoya) Report IPPJ-19 (1963).

18. R. S. Harp, G. S. Kino, and J. Pavkovich, Phys. Rev. Letters 11, 310 (1963).

19. J. Pavkovich and G. S. Kino, Aerospace Research Laboratories Report ARL 64-15 (1964).

20. J. M. Pavkovich, Aerospace Research Laboratories Report ARL 64-17 (1964).

21. R. Harp and G. S. Kino, Aerospace Research Laboratories Report ARL 64-14 (1964).

22. Y. H. Ichikawa, Comptes Rendus 256, 3434 (1963).

23. Y. H. Ichikawa, Nuclear Fusion (Japan) 11, 420 (1963) and Institute of Plasma Physics (Nagoya) Report IPPJ-14 (1963).

24. Y. H. Ichikawa, Nuclear Fusion (Japan) 11, 436 (1963); also Nihon Univ. Dept. of Physics Report NUP-63-14 and NUP-63-15 (1963).

25. J. Uramoto, H. Ikegami, and K. Takayama, Institute of Plasma Physics (Nagoya) Report IPPJ-15 (1963).

26. T. H. Y. Yeung and J. Sayers, Proc. Phys. Soc. 70B, 663 (1957).

27. D. C. Haycock and K. D. Baker, Electronics, Nov. 1962, p. 81.

28. A. Y. Wong, R. W. Motley, and N. D'Angelo, Phys. Rev. 133, A 436 (1964).

29. D. G. Bills, R. B. Holt, and B. T. McClure, J. Appl. Phys. 33, 29 (1962).

30. H. J. Oskam, R. W. Carlson, and T. Okuda, Physica 30, 182, 193, and 375 (1964); also Aeronautical Research Laboratories Report ARL-62-417 (1962) and J. Appl. Phys. 33, 3141 (1962).

31. K. Bol and J. Fujita, Princeton Plasma Physics Laboratory (private cummunication).

32. J. F. Waymouth, J. Appl. Phys. 30, 1404 (1959).

33. D. Kamke and H.-J. Rose, Z. Phys. 145, 83 (1956).

34. W. Koch, Phys. Z. 36, 855 (1935).

35. H. Beck, Z. f. physik 97, 355 (1935).

36. B. T. Barnes, Phys. Rev. 86, 351 (1952).

37. R. A. Ledrus, Appl. Sci. Research B5, 151 (1955).

38. J. Alexeff and R. Neidigh, Phys. Rev. Letters 7, 223 (1961).

39. C. Etievant and M. Perulli, Comptes Rendus 255, 2739 (1962).

40. R. W. Motley and N. D'Angelo, Phys. Fluids 6, 296 (1963).

41. See, for instance, J. O. Hinze, "Turbulence," McGraw-Hill Book Co., New York, 1959.

42. L. Spitzer, Jr., Phys. Fluids 3, 659 (1960); also Princeton University Project Matterhorn Tech Memo 50, NYO-7989 (1957).

43. H. W. Batten, H. L. Smith, and H. C. Early, J. Franklin Inst. 262, 17 (1956).

44. F. W. Crawford and J. D. Lawson, J. Nucl. Energy, Part C, 3, 179 (1961).

45. F. W. Crawford, J. Appl. Phys. 33, 15 (1962).

46. M. G. Rusbridge, D. J. Lees, and P. A. H. Saunders, Nuclear Fusion Supplement, Part 3, 895 (1962).

47. R. L. Bingham, F. F. Chen, and W. L. Harries, Princeton Plasma Physics Laboratory Report MATT-63 (1962).

48. F. F. Chen and A. W. Cooper, Phys. Rev. Letters 9, 333 (1962); Princeton Plasma Physics Laboratory Report MATT-140 (1962).

49. H. S. Rothman, H. Guthart, and T. Morita, Phys. Fluids 6, 1775 (1963).

50. L. Spitzer, Jr., Phys. Fluids 1, 253 (1958).

51. K. Bol, Phys. Fluids 7, (1964); Princeton Plasma Physics Laboratory Report MATT-224 (1963).

52. See, for instance, A. van der Ziel, "Noise," Chap. 12, Prentice-Hall, Inc., Englewood Cliffs, New Jersey, 1954.

## FIGURE CAPTIONS

Fig. 6.1 The shift of the $\ell n$ I - V curve due to an oscillation in probe potential. Note that the slope, which gives the temperature, is unchanged. (Garschadden and Emeleus, Ref. 1 ).

Fig. 6.2. The variation of average electron current in the transition region with amplitude of sinusoidal signal on the probe, illustrating the $I_o$ dependence predicted by theory. (Cairns, Ref. 6 ).

Fig. 6.3. Theoretical and experimental curves of average negative probe current for probes with a superimposed sinusoidal voltage of amplitude $\delta\eta\ kT_e/e$ extending into the saturation ion current region of the characteristic. (Boschi and Magistrelli, Ref. 3 ).

Fig. 6.4. Typical resonance probe curves of dc electron current vs. frequency of signal applied to the probe, for various amplitudes of signal. The plasma was a weak Hg discharge at $10^{-4}$ torr and a few mA of discharge current. (Ichikawa and Ikegami, Ref. 11 ).

Fig. 6.5. Dielectric slab model of a plasma and sheath, used for computing the current to a resonance probe.

Fig. 6.6. Equivalent circuit of a resonance probe system.

Fig. 6.7. RF and dc components of the current to a plane resonance probe in a low-density plasma, verifying the predictions of the dielectric slab model. (Uramoto et al., Ref. 17 ).

Fig. 6.8. Calculated and measured rf field amplitude in the neighborhood of an oscillating plane probe, for two values of the frequency. (Harp et al., Ref. 18 ).

Fig. 6.9. The relative rf signal transmitted between two probes as a function of frequency, showing a sharp minimum which gives the value of $\omega_p$. (Levitskii and Shashurin, Ref. 14 ).

Fig. 6.10. Schematic of the sheath potential distributions (a) and ion and electron density distributions (b) in the initial (1) and final (2) states when a negative probe is pulsed further negative. The shaded region in (b) represents the number of ions which must flow to the probe. The dashed curve (3) in (a) shows a potential profile during the transient state. The dotted curve (4) shows a transient state when the probe is pulsed back from $V_2$ to $V_1$.

Fig. 6.11. Schematic of the variation in time of the displacement current $j_d$, the ion conduction current $j_i$, and the total probe current $j_t$ when the probe potential is pulsed from $V_1$ to $V_2$ and back again. Note that the equilibrium current at $V_2$ may be higher than that at $V_1$ if the sheath area changes because of finite geometry.

Fig. 6.12. Schematic of the density and potential distributions in the initial (solid) and transient (dashed) states of the sheath around a spherical or cylindrical pulsed positive probe.

Fig. 6.13. Schematic of the response of a positive probe to a square pulse of probe potential.

Fig. 6.14. Example of the frequency spectrum of oscillations in floating potential of a probe in a discharge in a strong magnetic field. The data were taken in a hot-cathode reflex discharge in 5 microns of He and 2000 gauss; the plasma density was of order $2 \times 10^{12}$ cm$^{-3}$. Note that the vertical scale is logarithmic. (Chen et al., Refs. 47 and 48).

Fig. 6.15. Examples of the variation of the correlation coefficients $\hat{R}(\xi, 0)$ with probe separation $\xi$ for frequency-selected signals. The curves are for different distributions of wave number k: (a) a single value of k; (b) a uniform distribution of k between 0 and k; (c) a Gaussian distribution of k about k, with spread $\Delta k = 0.1\, k$; (d) a resonance-type distribution with $\Delta k = 0.2\, k$; (e) a Gaussian distribution with $\Delta k = k$; and (f) a resonance-type distribution with $\Delta k = k$.

Fig. 6.16. The effect of a time-delay $\tau$ on the correlation coefficient $\hat{R}(\xi, \tau)$ for (A) unidirectional waves and (B) standing waves.

Fig. 6.17. The function $\hat{R} = (1 - P)/(1 + P)$ used for computing the correlation coefficient from measured ratios of the mean square sum and difference signals.

Fig. 6.18. Block diagram of circuit used for measuring correlation coefficients for density fluctuations. (Bol, Ref. 51 ).

Fig. 6.19. Typical results for azimuthal correlation measurements in a stellarator discharge in $10^{-3}$ torr of He. The bars indicate the maximum value of $\hat{R}(\xi, \tau)$ obtainable by varying $\tau$ at a given value of $\xi$ ; the fact that this value falls on the envelope of $\hat{R}(\xi, 0)$ indicates that the waves are unidirectional. (Bol, Ref. 51 ).

Fig. 6.20. Typical results for longitudinal correlation measurements in a reflex arc in $10^{-2}$ torr of He . This shows that at high magnetic fields the fluctuations in density are well-correlated along the field. (Chen and Cooper, Ref. 48 ).

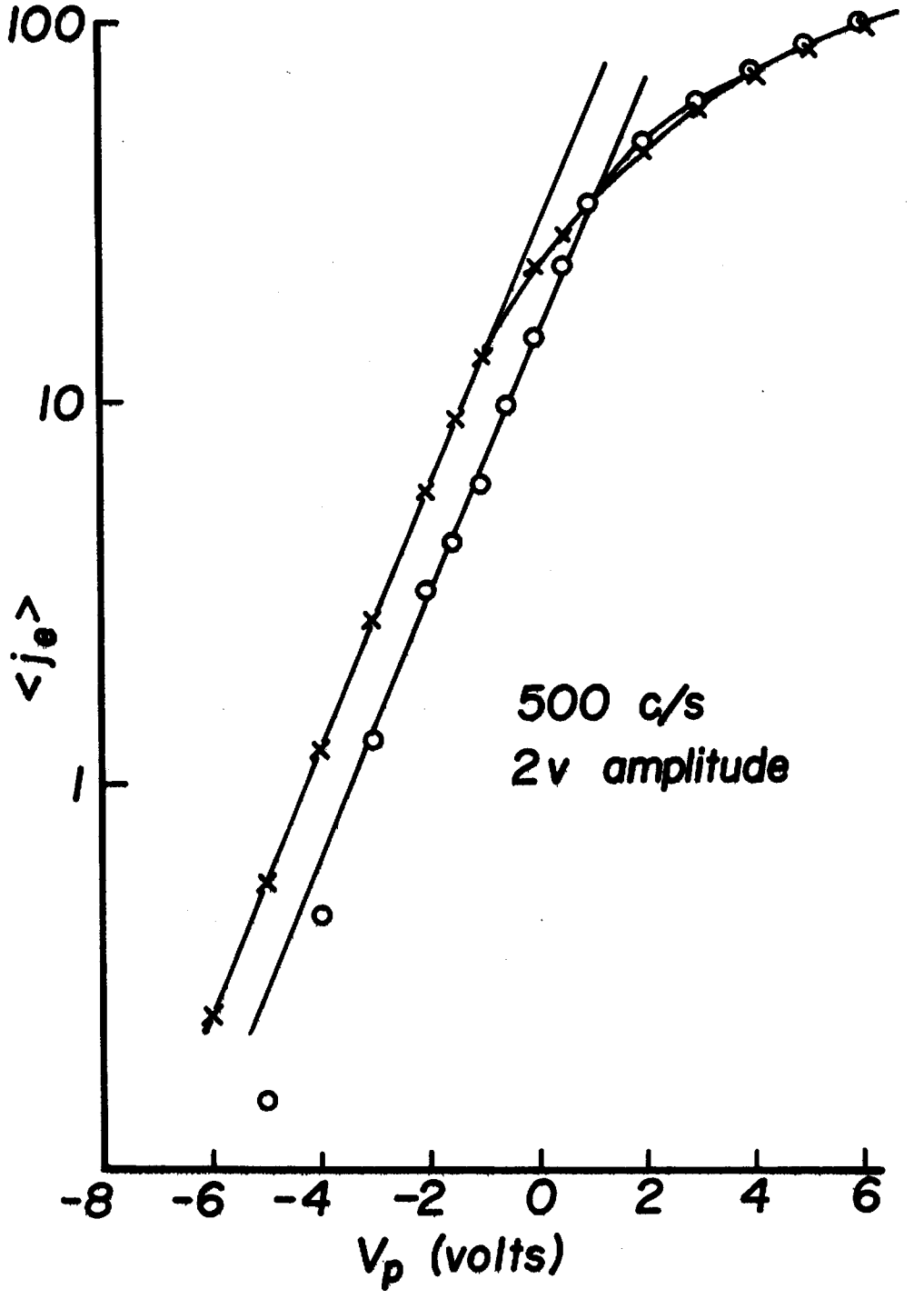
100
10
1
$\langle j_e \rangle$
500 c/s
2v amplitude
-8
-6
-4
-2
0
2
4
6
$V_p$ (volts)

643330

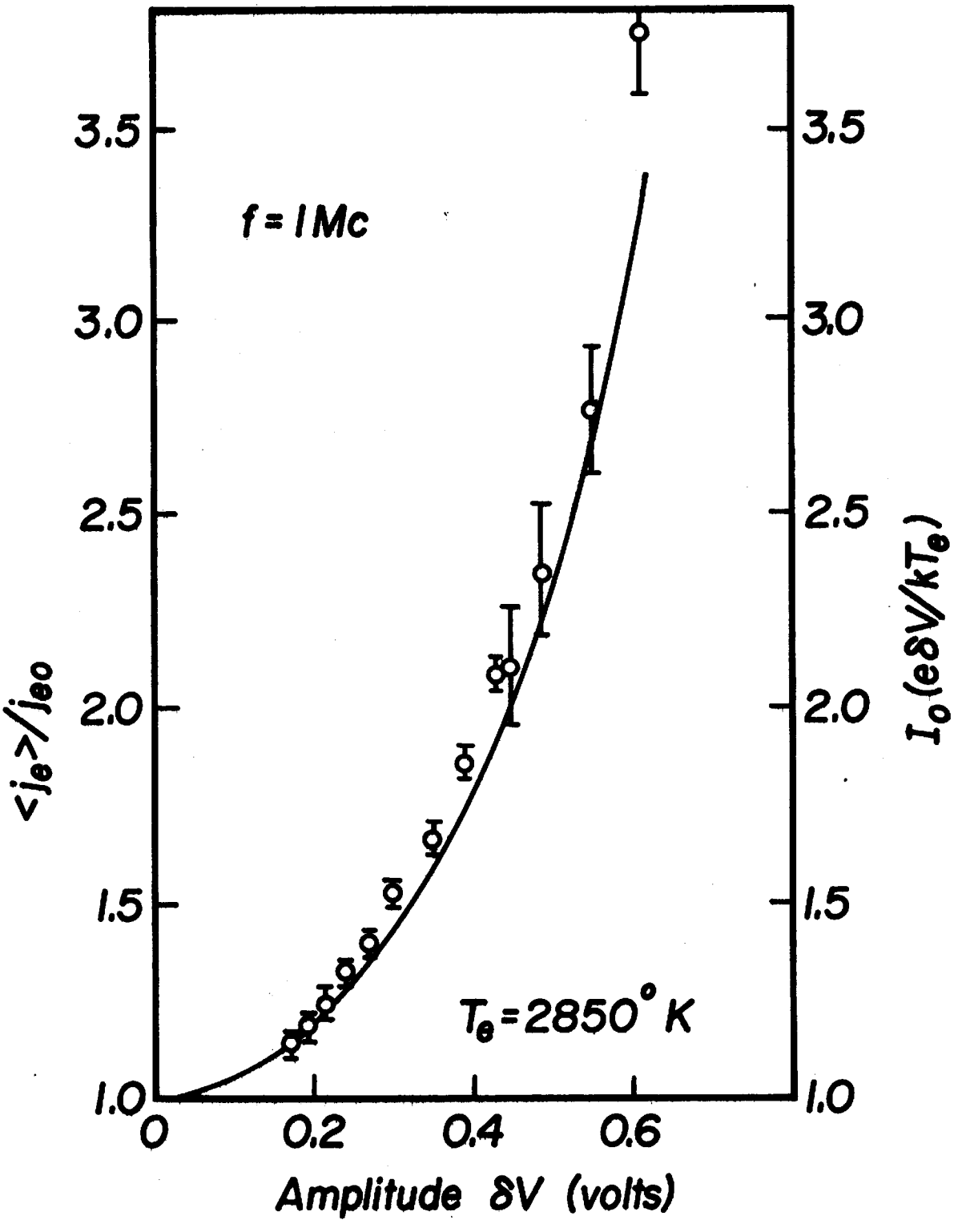
f = 1 Mc
$T_e = 2850^\circ K$
$\langle j_e \rangle / j_{eo}$
$I_o(e\delta V/kT_e)$
Amplitude δV (volts)
1.0
1.5
2.0
2.5
3.0
3.5
0
0.2
0.4
0.6

643327

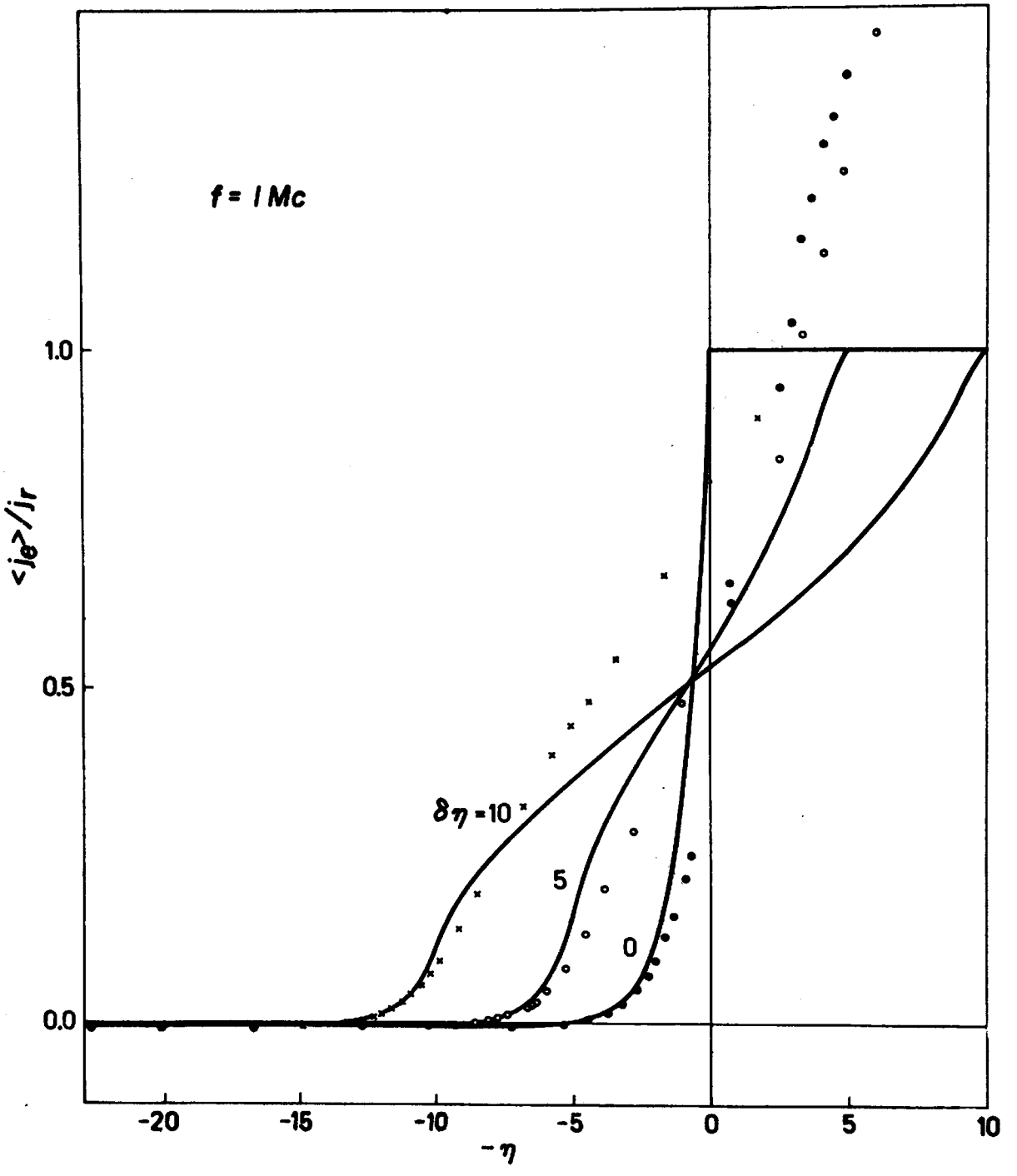


643328

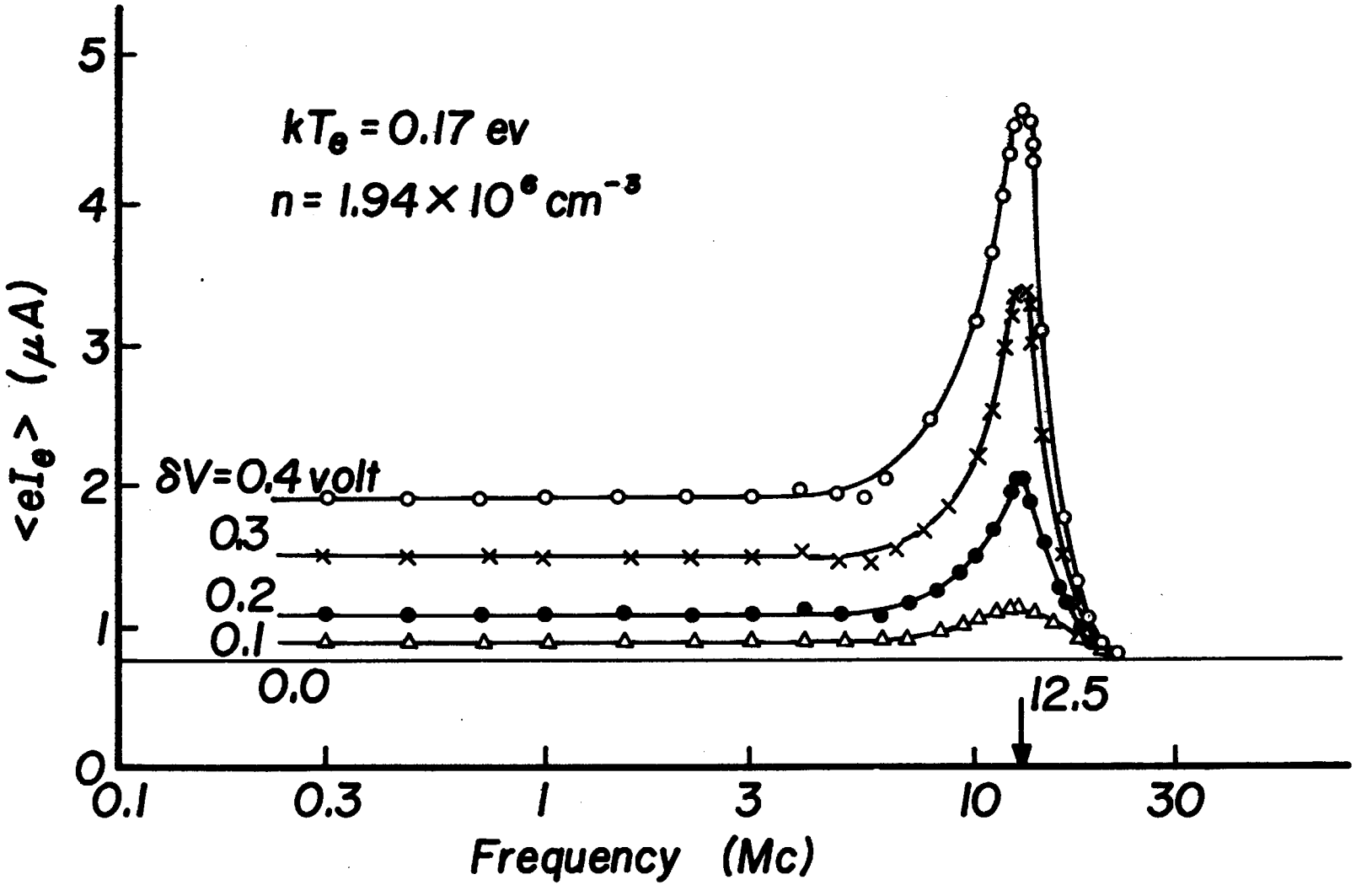
$kT_e = 0.17$ ev
$n = 1.94 \times 10^6$ cm$^{-3}$
$\langle eI_e \rangle$ ($\mu$A)
δV=0.4 volt
0.3
0.2
0.1
0.0
12.5
0
1
2
3
4
5
0.1
0.3
1
3
10
30
Frequency (Mc)

643329

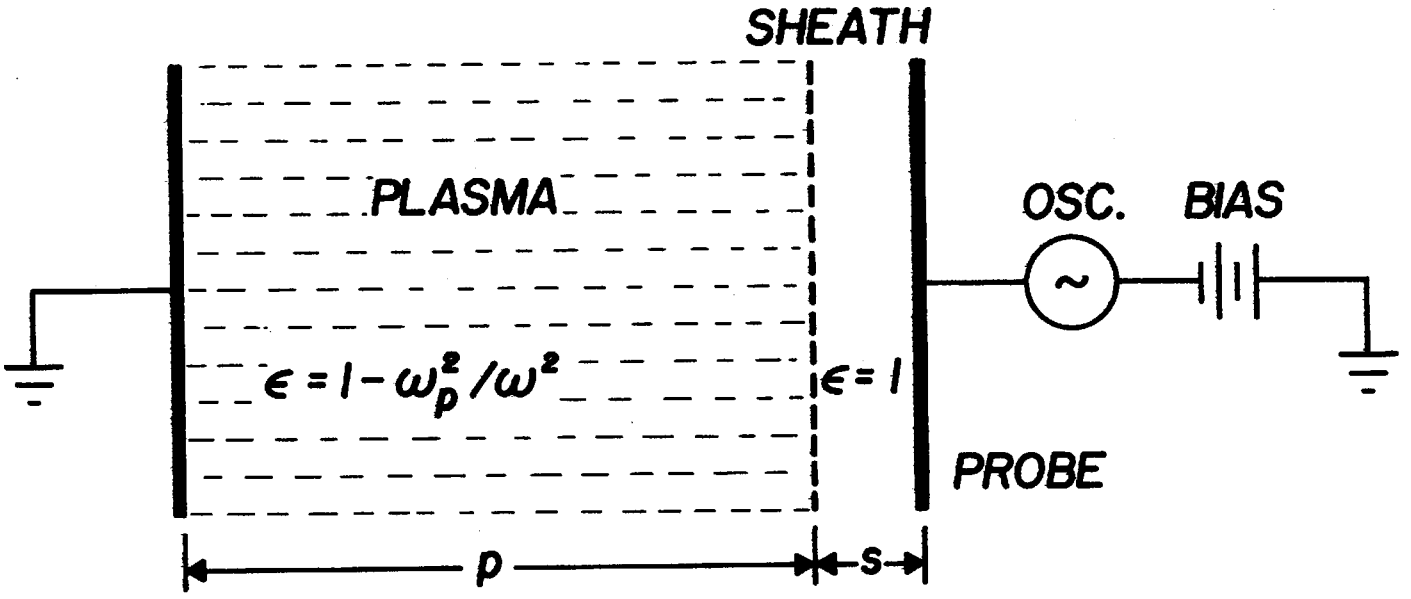
SHEATH
PLASMA
$\epsilon = 1 - \omega_p^2/\omega^2$
$\epsilon = 1$
OSC.
BIAS
PROBE
p
s
643399

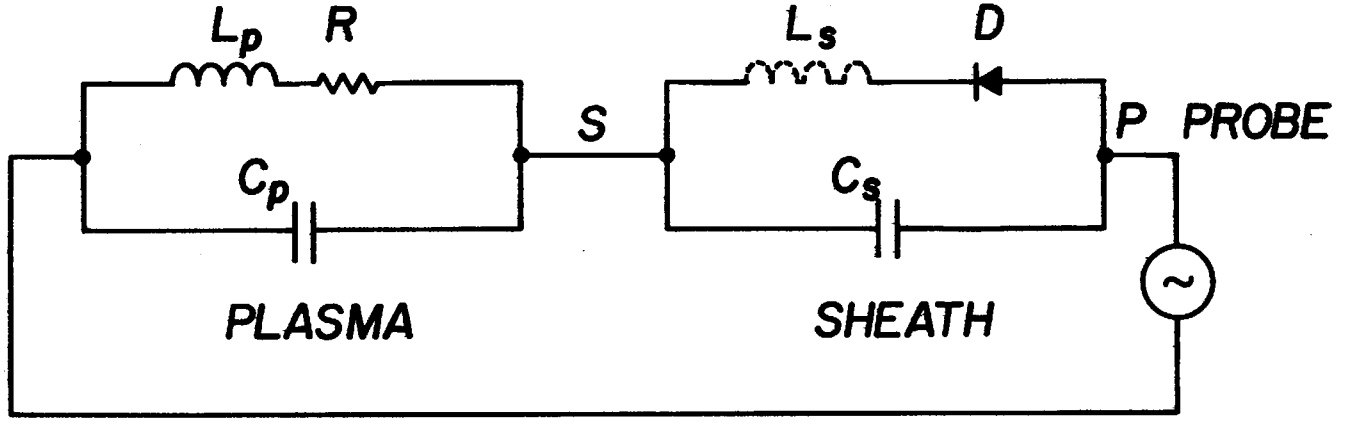


643396

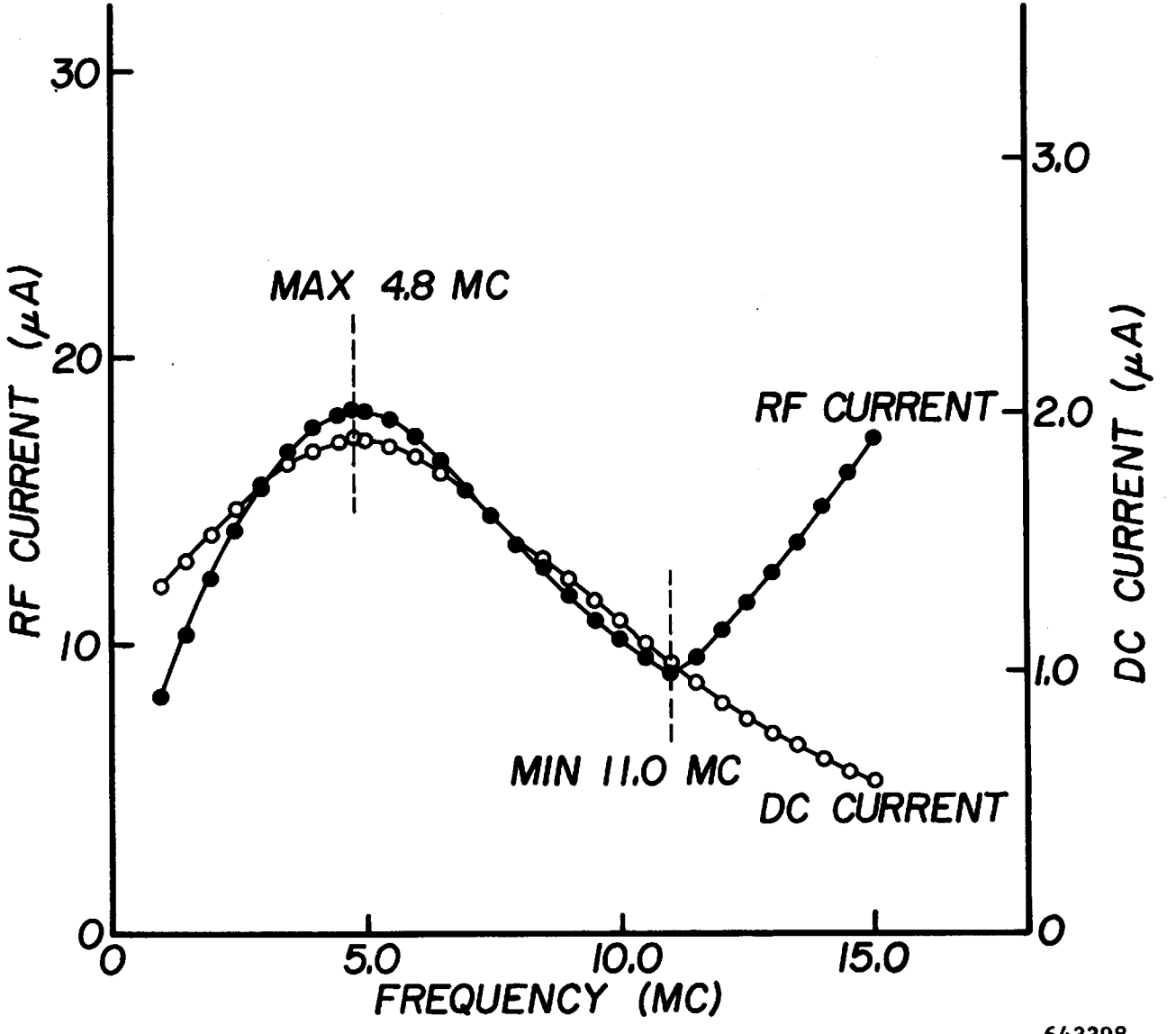
30
20
10
0
RF CURRENT (μA)
3.0
2.0
1.0
0
DC CURRENT (μA)
MAX 4.8 MC
MIN 11.0 MC
RF CURRENT
DC CURRENT
0
5.0
10.0
15.0
FREQUENCY (MC)
643398

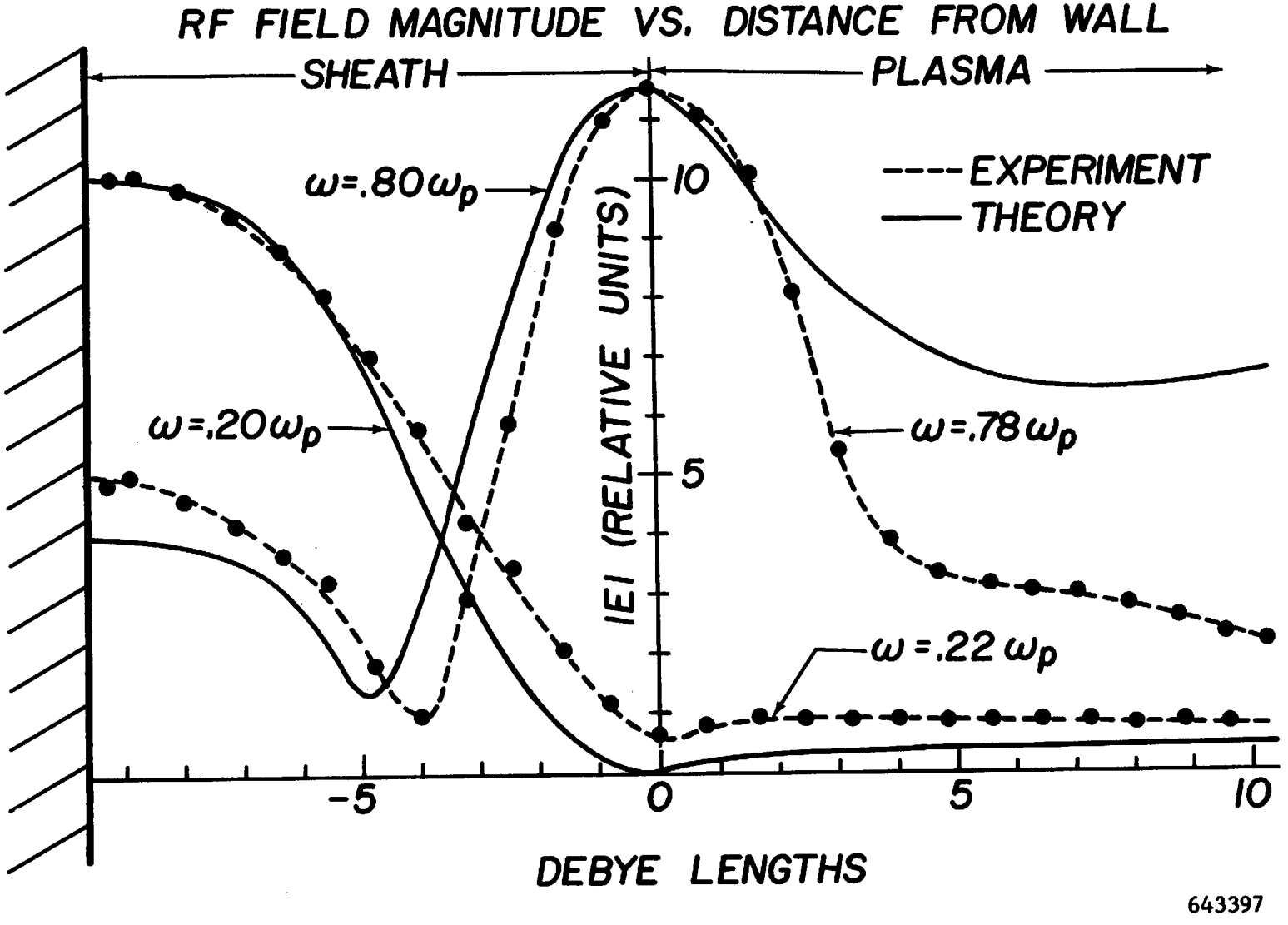
RF FIELD MAGNITUDE VS. DISTANCE FROM WALL
SHEATH
PLASMA
EXPERIMENT
THEORY
ω=.80ωp
ω=.20ωp
ω=.78ωp
ω=.22ωp
|E| (RELATIVE UNITS)
10
5
-5
0
5
10
DEBYE LENGTHS
643397

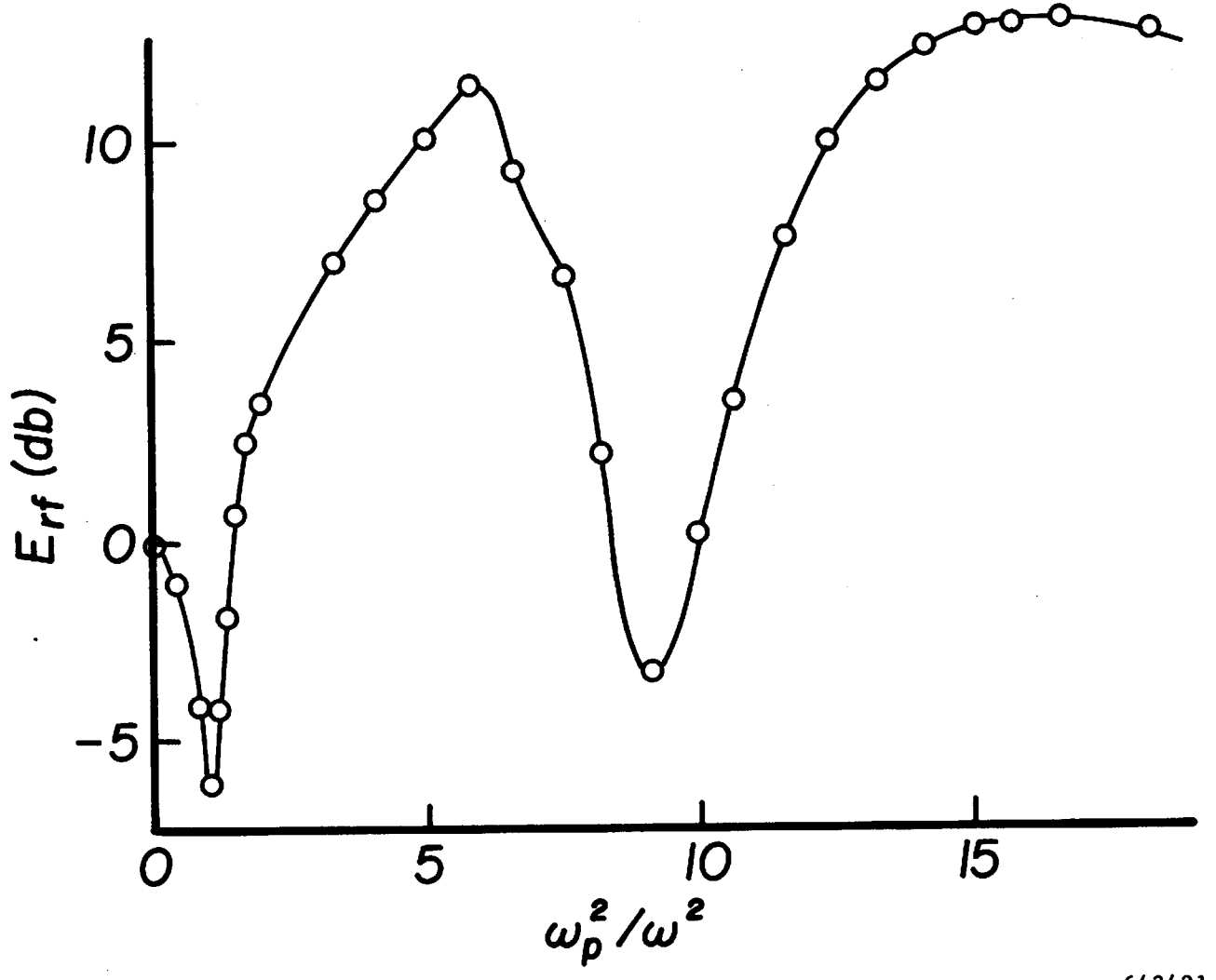


643421

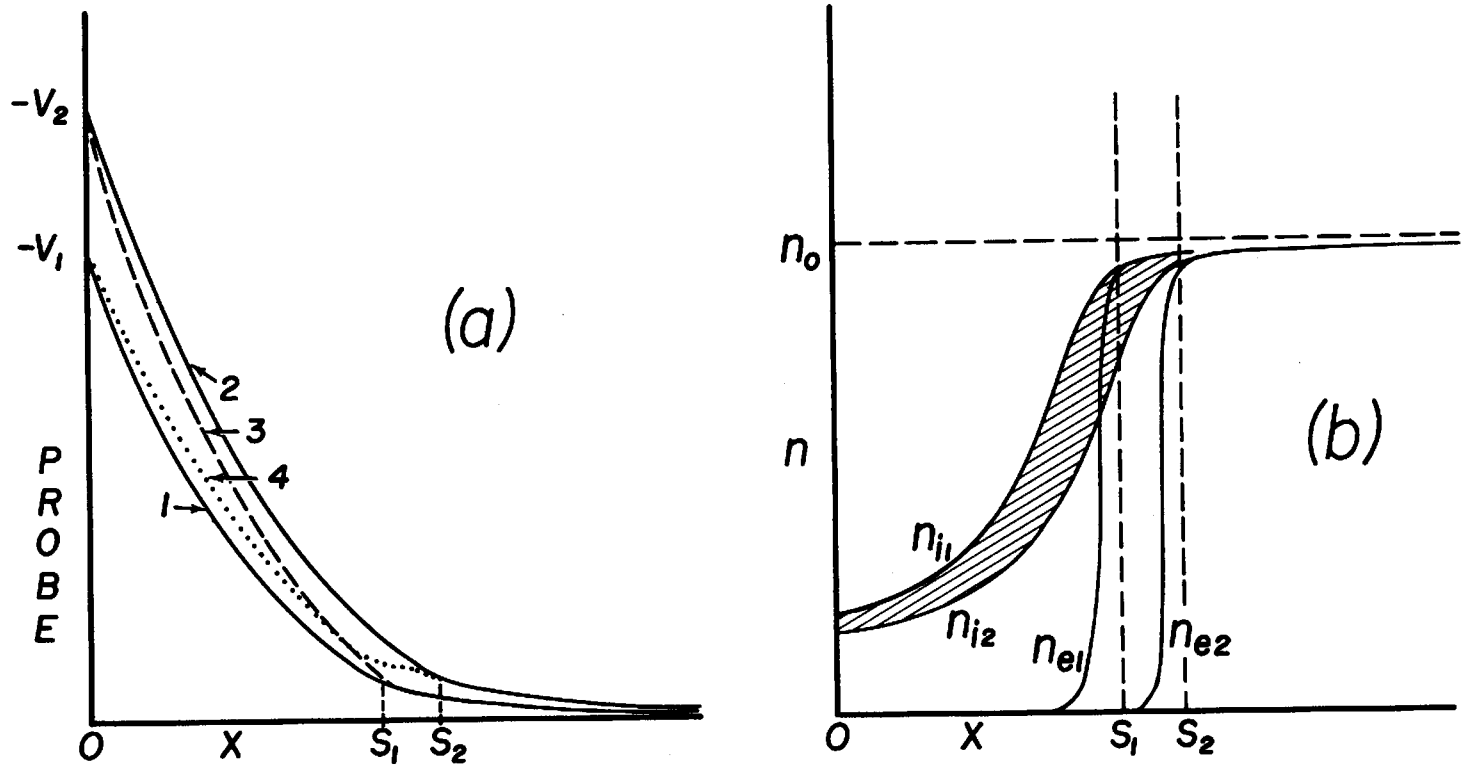
-V2
-V1
PROBE
(a)
2
3
4
1
O
X
S1
S2
n0
n
(b)
ni1
ni2
ne1
ne2
O
X
S1
S2
643390

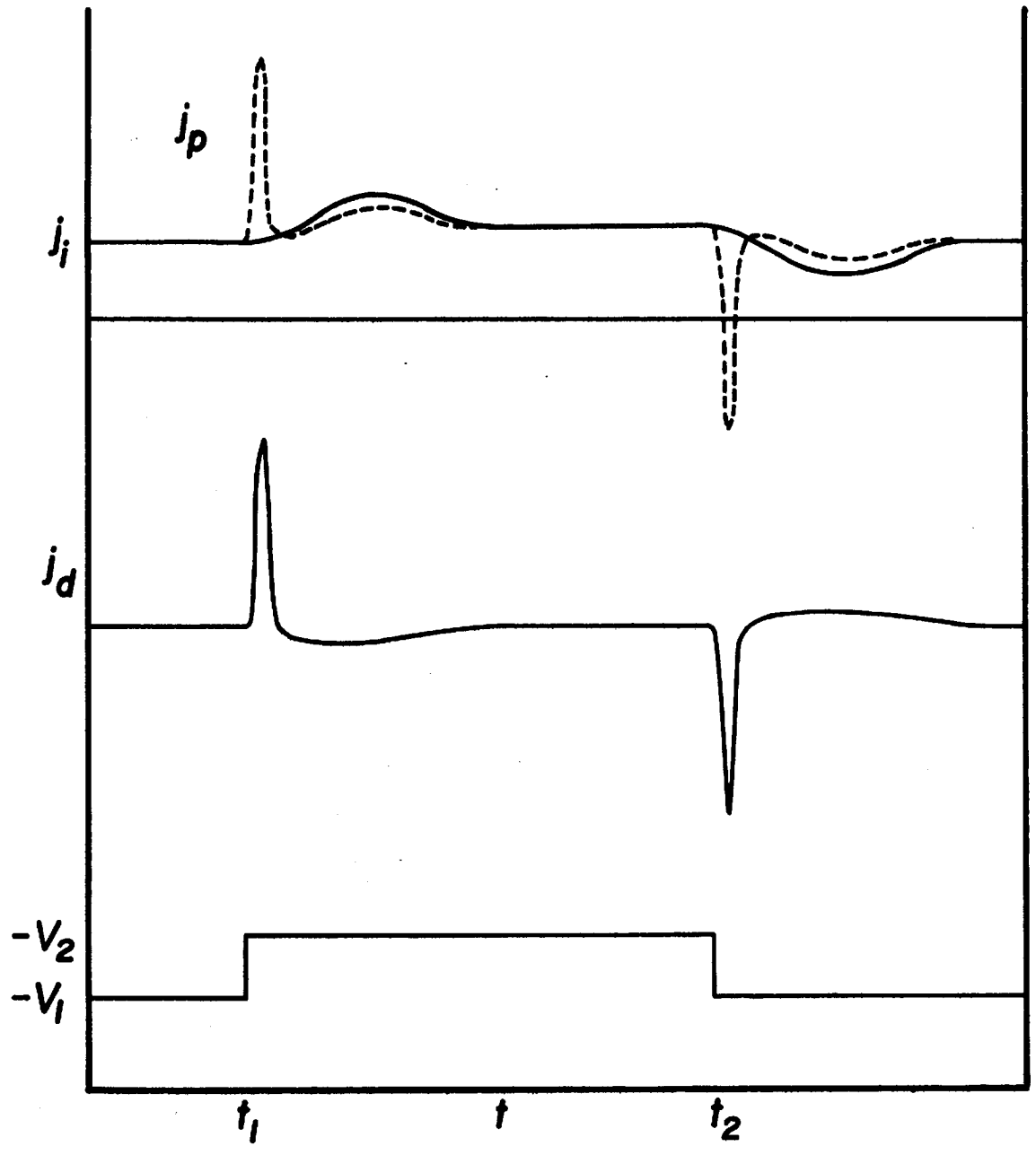


643392

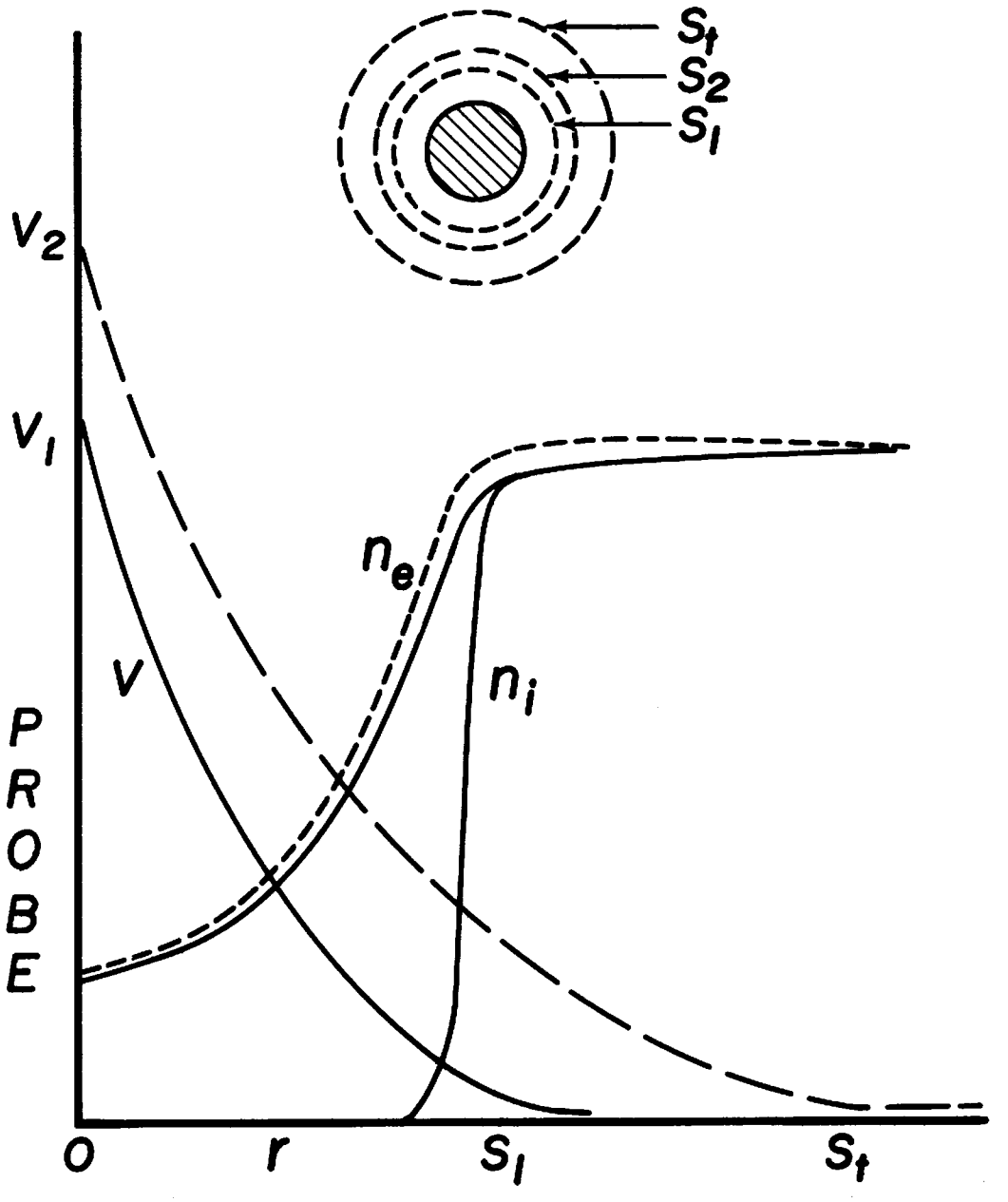


643393

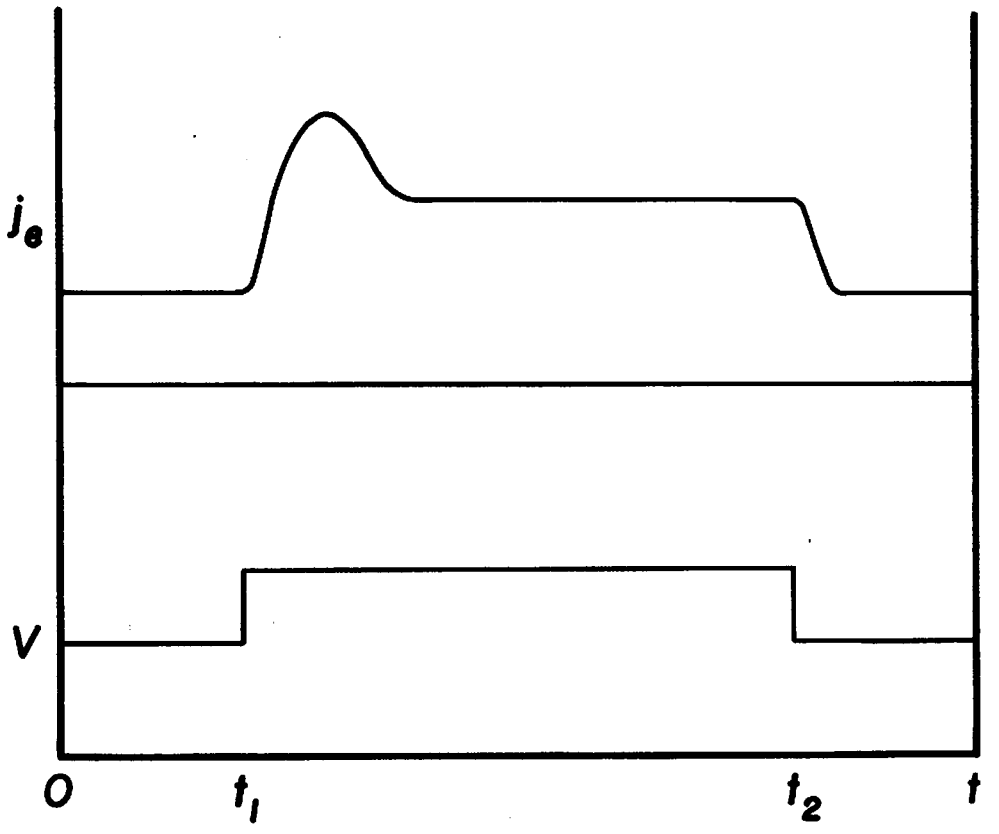
$j_e$
V
O
$t_1$
$t_2$
t
643394

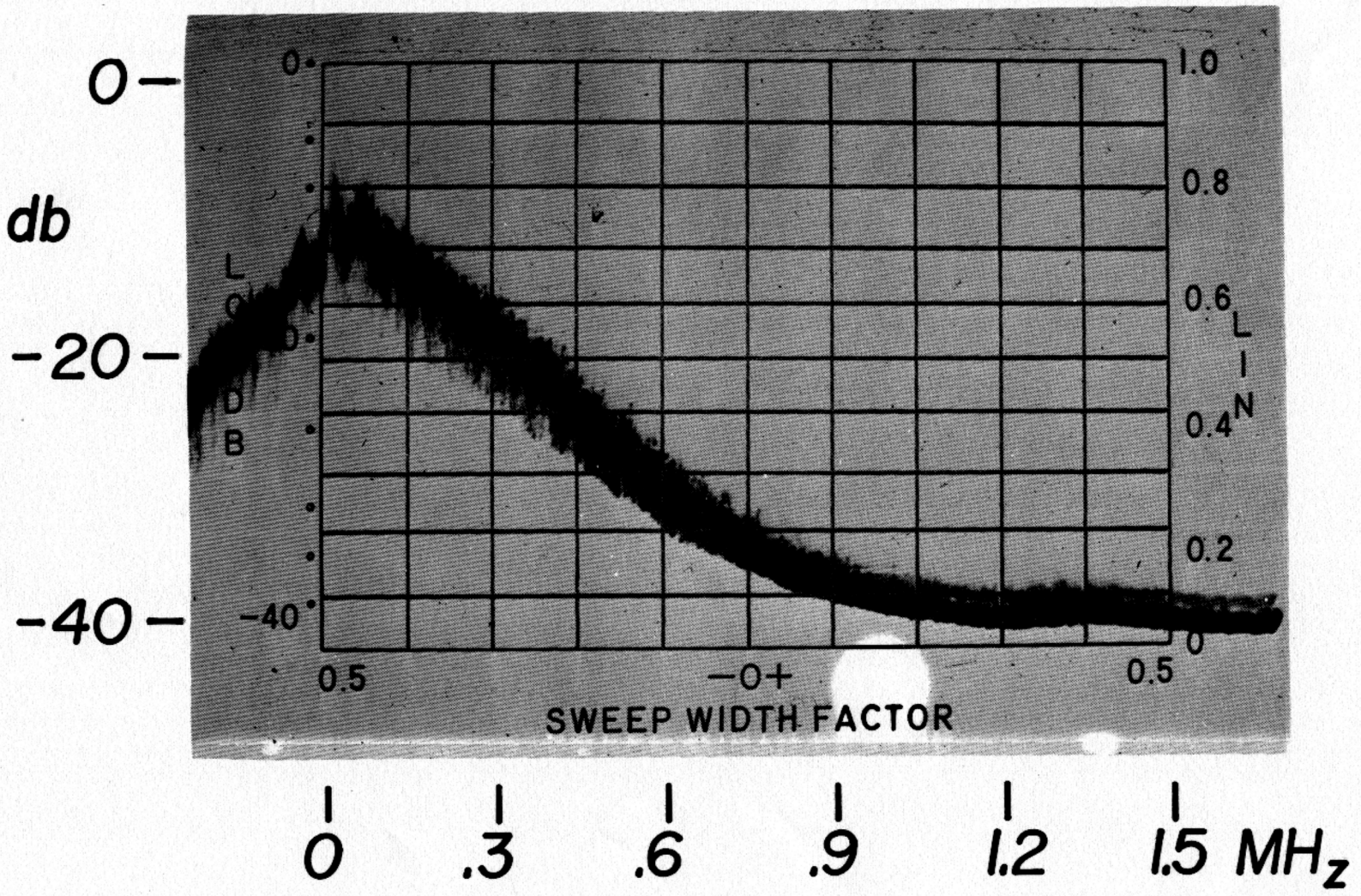
0
db
-20
-40
0
-40
LOG DB
1.0
0.8
0.6
LIN
0.4
0.2
0
0.5
0
0.5
SWEEP WIDTH FACTOR
0
.3
.6
.9
1.2
1.5 MHz
643422

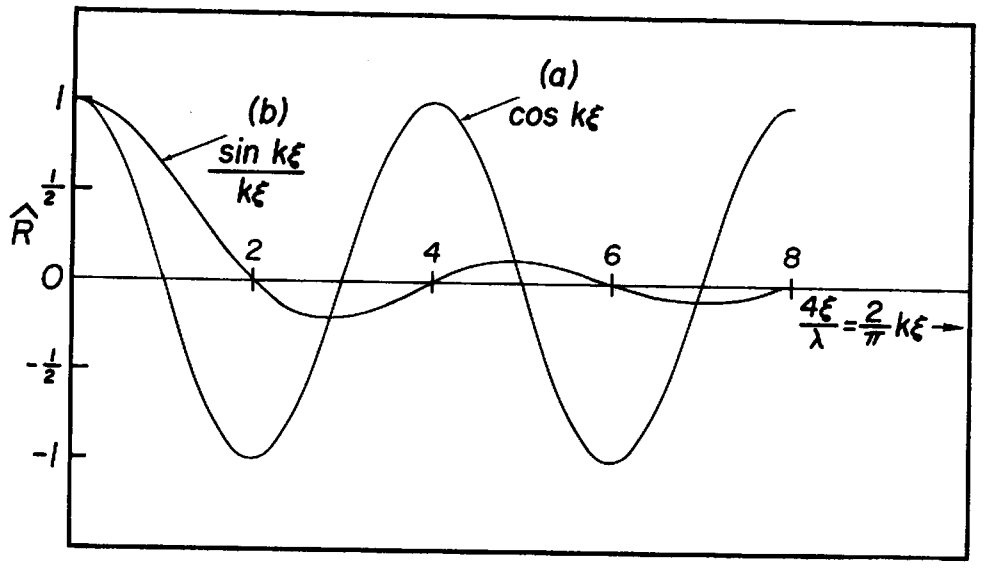
(a)
cos kξ
(b)
sin kξ / kξ
1
1/2
0
-1/2
-1
2
4
6
8
4ξ/λ = 2/π kξ

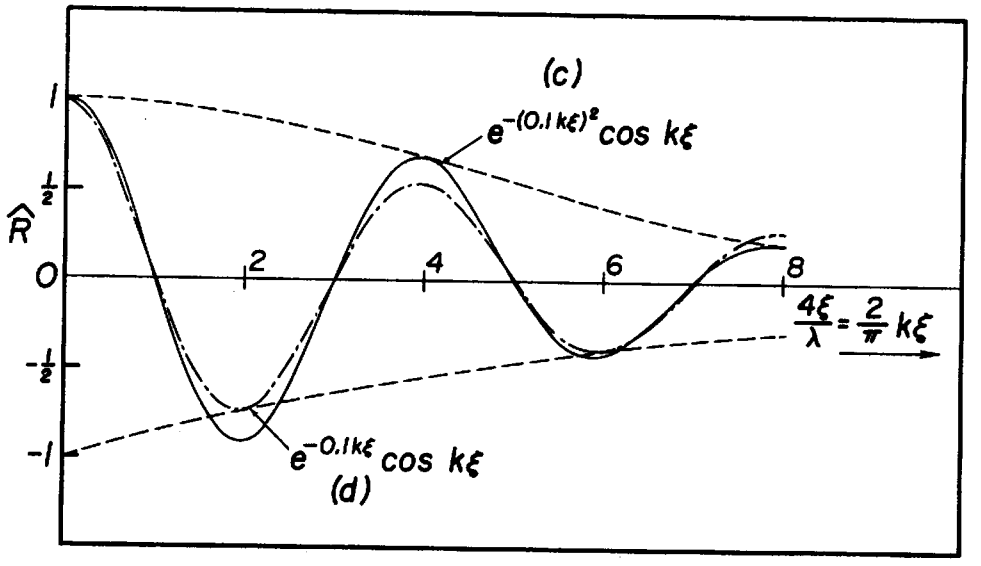
(c)
e^-(0.1 kξ)^2 cos kξ
1
1/2
0
-1/2
-1
2
4
6
8
4ξ/λ = 2/π kξ
e^-0.1kξ cos kξ
(d)

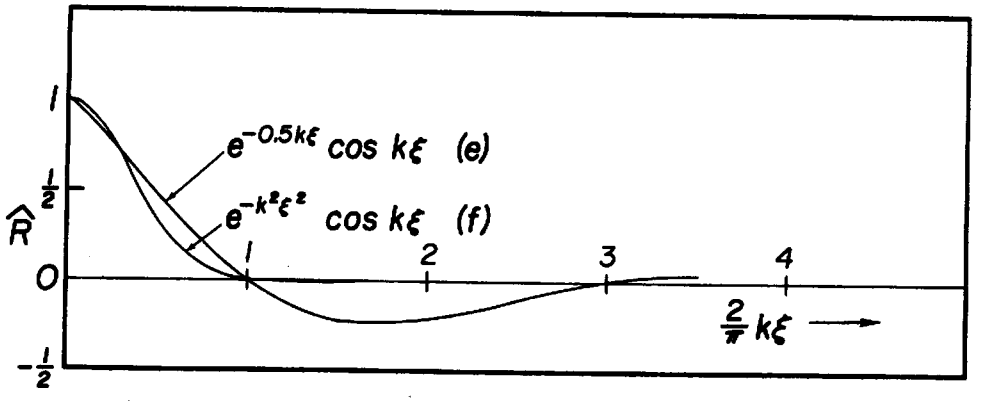
e^-0.5kξ cos kξ (e)
e^-k^2ξ^2 cos kξ (f)
1
1/2
0
-1/2
1
2
3
4
2/π kξ

643387

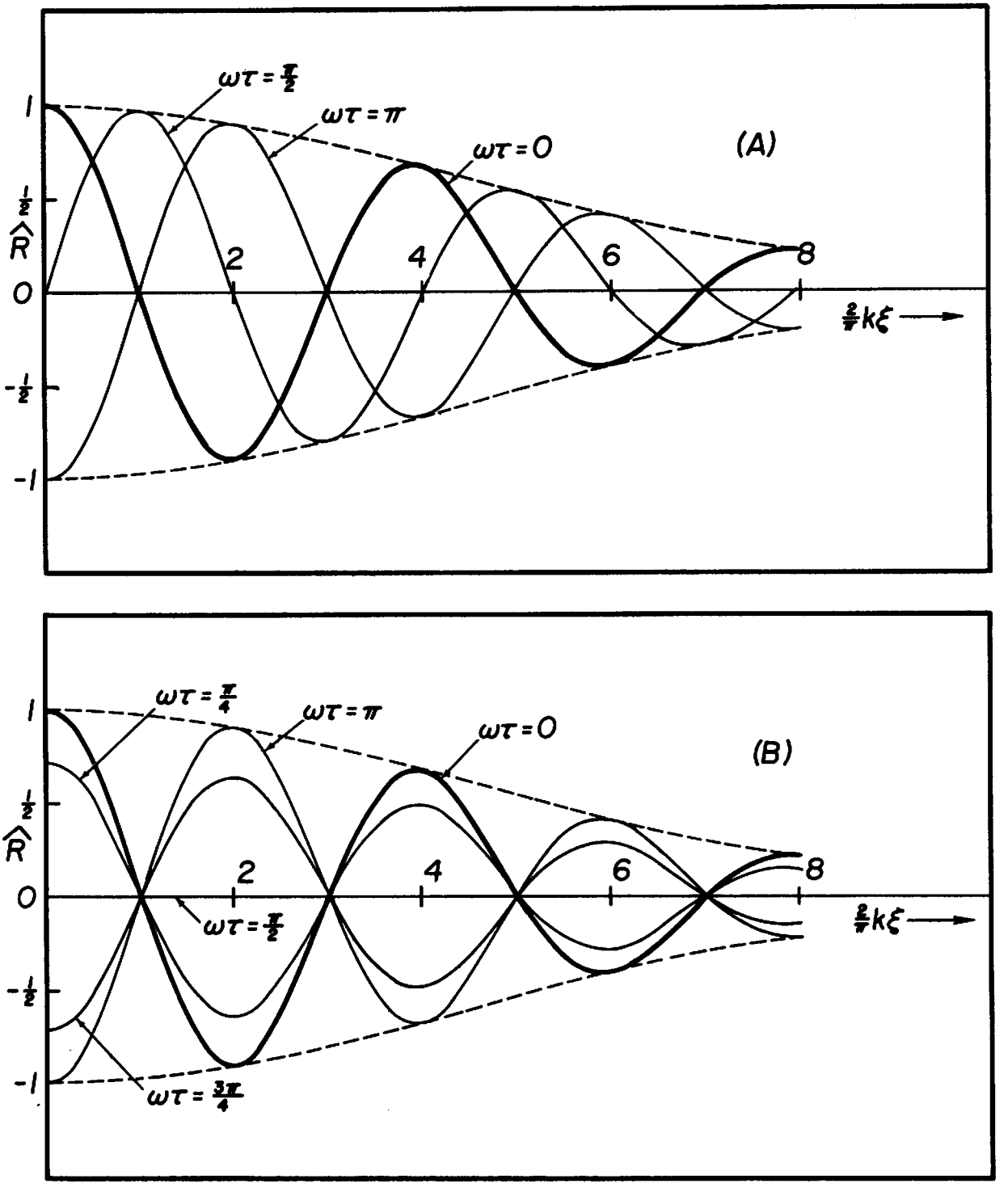
$\omega\tau = \frac{\pi}{2}$
$\omega\tau = \pi$
$\omega\tau = 0$
(A)
1
$\frac{1}{2}$
$\hat{R}$
0
$-\frac{1}{2}$
-1
2
4
6
8
$\frac{2}{\pi}k\xi$
$\omega\tau = \frac{\pi}{4}$
$\omega\tau = \pi$
$\omega\tau = 0$
(B)
$\omega\tau = \frac{\pi}{2}$
$\omega\tau = \frac{3\pi}{4}$

643389

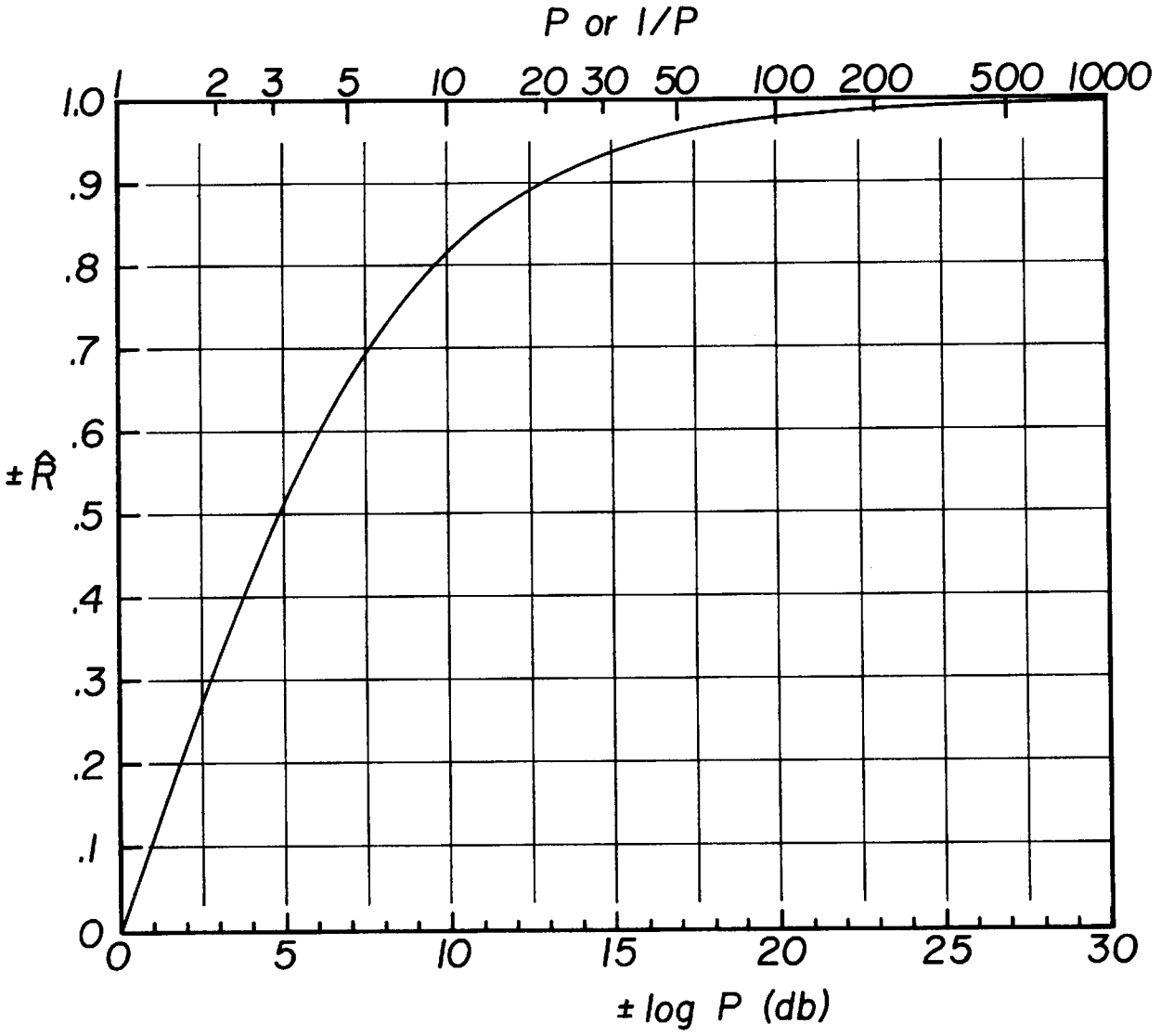
P or 1/P
1
2
3
5
10
20
30
50
100
200
500
1000
1.0
.9
.8
.7
.6
.5
.4
.3
.2
.1
0
± R̂
0
5
10
15
20
25
30
± log P (db)

643388

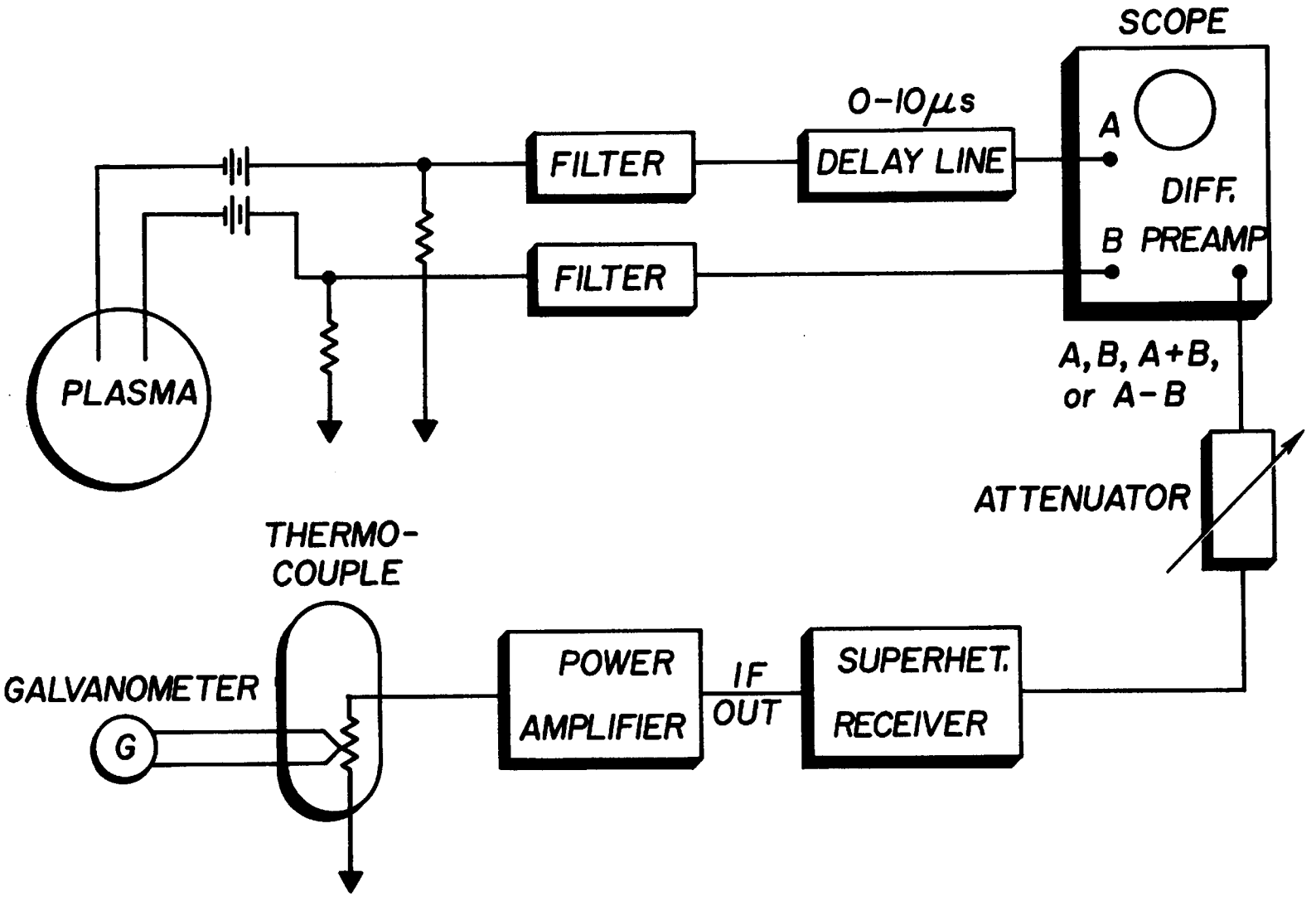
SCOPE
0-10μs
A
DIFF.
B PREAMP
FILTER
DELAY LINE
FILTER
PLASMA
A, B, A+B,
or A-B
ATTENUATOR
THERMO-
COUPLE
GALVANOMETER
G
POWER
AMPLIFIER
IF
OUT
SUPERHET.
RECEIVER
643395

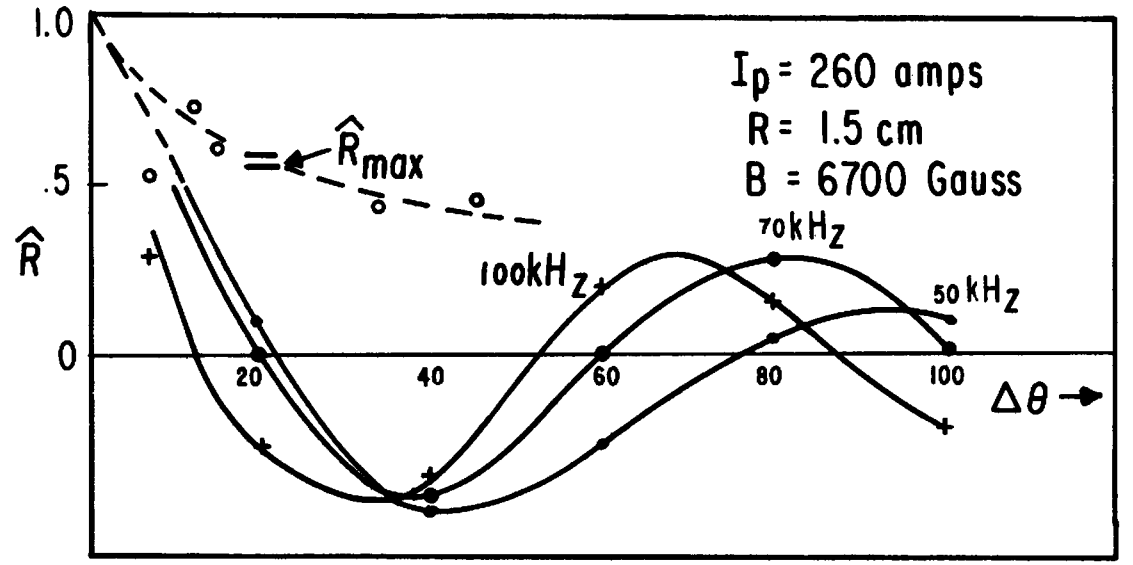


(a)

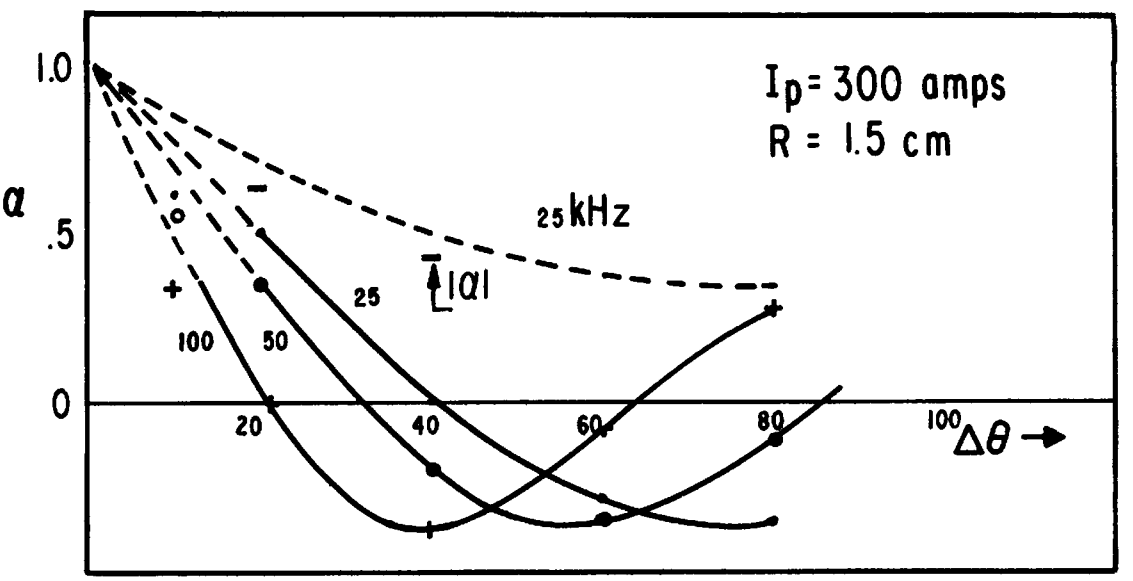


(b)

CORRELATION vs PROBE SEPARATION

643391

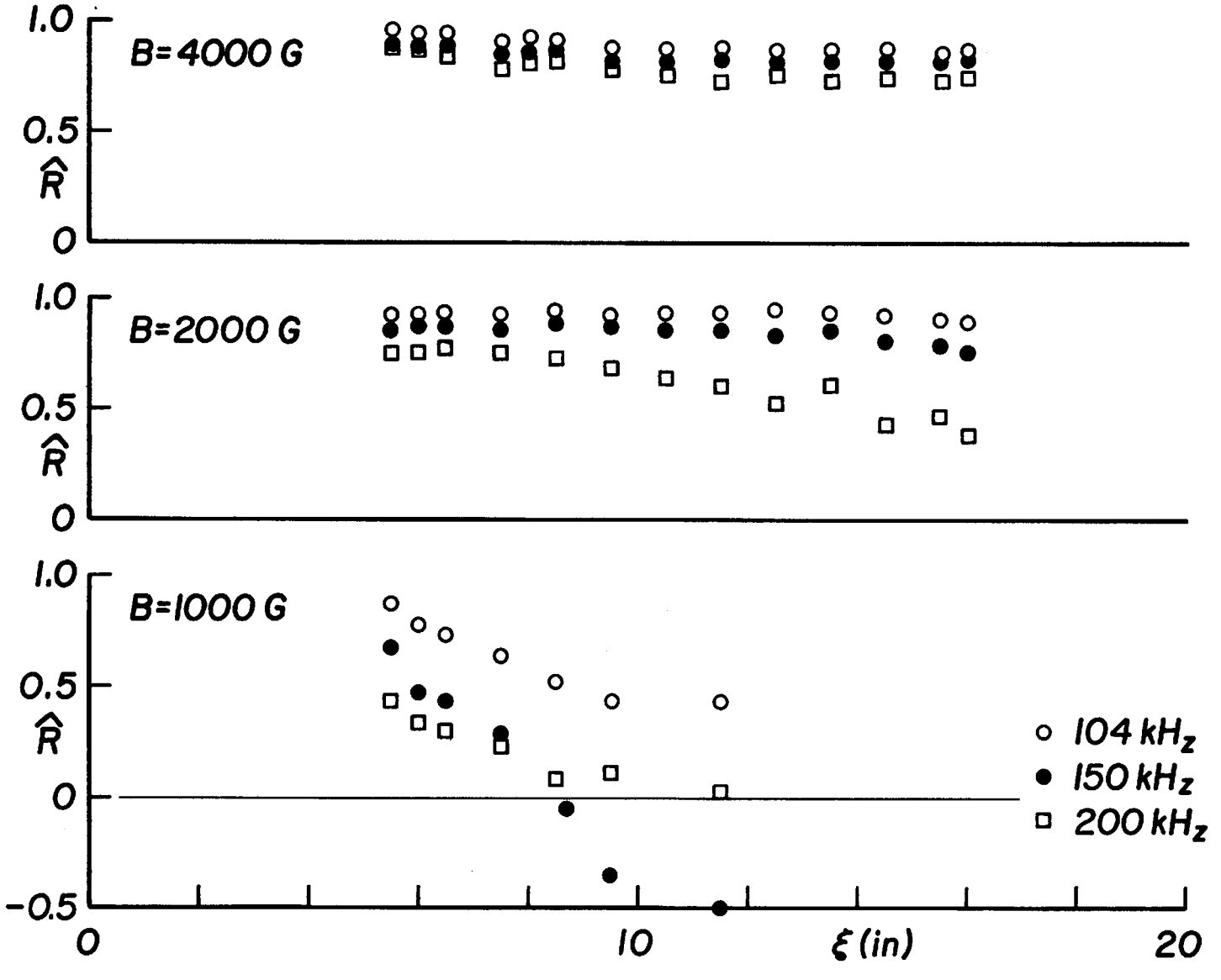
1.0
B=4000 G
0.5
$\hat{R}$
0
1.0
B=2000 G
0.5
$\hat{R}$
0
1.0
B=1000 G
0.5
$\hat{R}$
0
-0.5
0
10
ξ (in)
20
104 kHz
150 kHz
200 kHz

643386